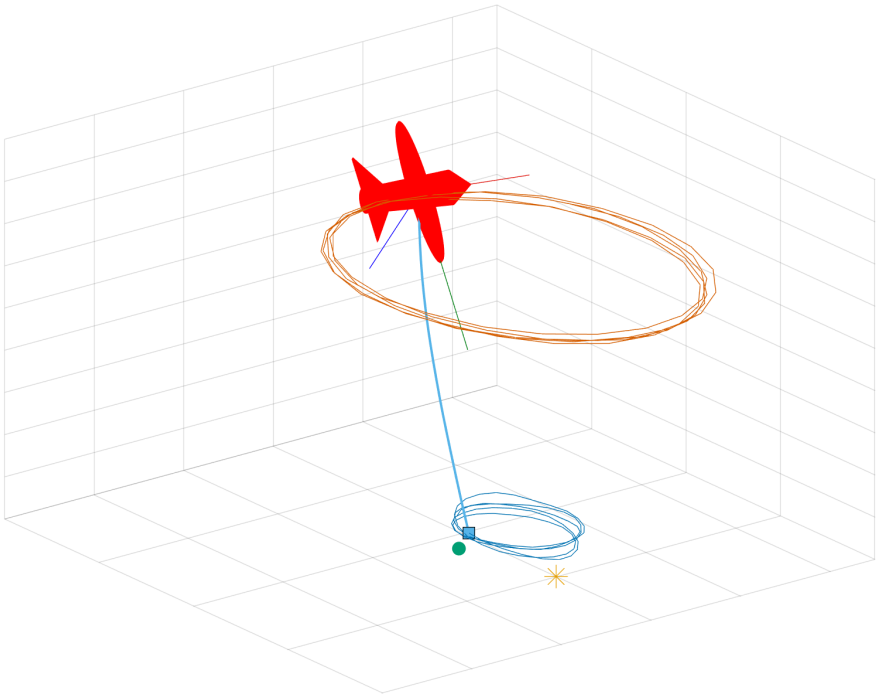

Fixed-wing UAVs in Windy Environments: A Circular Delivery System

Disturbance Prediction and Compensation Mechanisms

Master's thesis in Complex Adaptive Systems

ANTON CARLSSON
HUGO RÅDEGÅRD

DEPARTMENT OF ELECTRICAL ENGINEERING
CHALMERS UNIVERSITY OF TECHNOLOGY
Gothenburg, Sweden 2025
www.chalmers.se

Master's thesis 2025

Fixed-wing UAVs in Windy Environments: A Circular Delivery System

Disturbance Prediction and Compensation Mechanisms

Anton Carlsson
Hugo Rådegård

CHALMERS
UNIVERSITY OF TECHNOLOGY

Department of Electrical Engineering
Division of Systems and Control
Chalmers University of Technology
Gothenburg, Sweden 2025

Fixed-wing UAVs in Windy Environments: A Circular Delivery System
Disturbance Prediction and Compensation Mechanisms
ANTON CARLSSON, HUGO RÅDEGÅRD

Supervisor: Fredrik Falkman, Swedish Sea Rescue Society
Examiner: Balázs Adam Kulcsár, Department of Electrical Engineering

Master's Thesis 2025
Department of Electrical Engineering
Division of Systems and Control
Chalmers University of Technology
SE-412 96 Gothenburg
Telephone +46 31 772 1000

Cover: The circular delivery method in progress, simulated in Matlab, showing the path of the drone and the package, as it circles over the target.

Typeset in LaTeX
Printed by Chalmers Reproservice
Gothenburg, Sweden 2025

Fixed-wing UAVs in Windy Environments: A Circular Delivery System
Disturbance Prediction and Compensation Mechanisms
ANTON CARLSSON
HUGO RÅDEGÅRD
Department of Electrical Engineering
Chalmers University of Technology

Abstract

In some situations, when delivering packages with a fixed-wing UAV, a better accuracy is necessary than can be achieved with a fly-by drop. One alternative method is to circle close to the target point with the package suspended below the UAV with a rope. Through simulations it is shown that this circular method can deliver packages with a higher precision than can be done with the fly-by method. In steady wind conditions, it is proven possible to get a close estimation for where the package would land, were it to be released. This is done by a combination of an analytical solution to a system of differential equations in conjunction with a disturbance function based on previous simulations. In isolation, the impact of the turbulence can be minimized by releasing the package from as low a height as possible, and with a low relative velocity between the wind and the package in the horizontal plane at release. Contrary to that, when combining the estimation with the circular delivery method, the headwind releases gives a higher accuracy. For headwind drops the algorithm can land within 1 m of the target approximately 94 to 95 % of the time for wind velocities up to 10 m/s. This is significantly better than the fly-by algorithm, which can with 95 % certainty land only within 4 m of the target for a similar wind. For even stronger winds the accuracy decreases and for 15 m/s wind the circular algorithm can land within one meter with approximately 61 to 69 % probability. Compared to the fly-by, the package also has a lower velocity when it lands, when released with the circular delivery method. The 95th-percentile velocities are 9 m/s and 8 m/s respectively. One drawback with the circular algorithm, however, is that it takes longer time before the package is released, with an approximate time of 3 min on average compared to 10 s for the fly-by.

Keywords: UAV, fixed-wing, circular delivery, simulation, wind, turbulence, rope, towing.

Acknowledgements

We would like to extend our gratitude to our examiner, Balázs Adam Kulcsár, for listening and providing valuable input on our methods and results. We would also like to thank our supervisor, Fredrik Falkman, for his ideas and dedication to the project.

Anton Carlsson & Hugo Rådegård, Gothenburg, May 2025

List of Acronyms

Below is the list of acronyms that have been used throughout this thesis listed in alphabetical order:

CDF	Cumulative Distribution Function
ENU	East-North-Up (coordinate system)
NED	North-East-Down (coordinate system)
PID	Proportional–Integral–Derivative (controller)
SMHI	Swedish Meteorological and Hydrological Institute
SSRS	Swedish Sea Rescue Society
UAV	Unmanned Aerial Vehicle

Nomenclature

Below is the nomenclature of indices, sets, parameters, and variables that have been used throughout this thesis.

Indices

N	North direction
E	East direction
D	Down direction
$long$	Longitudinal direction (body-fixed coordinate system)
lat	Latitudinal direction (body-fixed coordinate system)
$vert$	Vertical direction (body-fixed coordinate system)
par	Direction parallel to the velocity of the package
ort	Direction orthogonal to the velocity of the package
g	Relative to the ground (of velocity)
a	Relative to the air (of velocity)
t	Relating to the turbulence
ana	Relating to the analytical estimation
$dist$	Relating to the disturbance function

Parameters

g	Gravitational constant
ρ_{air}	Air density
m	Mass of the package
d	Diameter of the package
A	Cross section area of the package
C_D	Drag constant

α	Shear constant
z_{ref}	Reference height for the wind
Ω	Spatial frequency of turbulence
ω	Angular spacial frequency of turbulence
Φ	Turbulence single-sided spectral density
σ	Turbulence intensity
L	Turbulence scale length
p	Angular turbulence rate
b	Wingspan
V	Drone airspeed ($\|\vec{v}_a\|$)
$\vec{I}$	Continuous indices in disturbance function
$\vec{F}$	The element-wise floor of $\vec{I}$
D	Discreet derivatives in disturbance function
E	Stored errors from pre-run simulations
P	Predicted error in one direction from disturbance function
$\vec{e}$	Estimated landing error
$\vec{p}$	Position of package
$\vec{d}$	Desired drop point
$\vec{s}$	Estimated movement during fall

Variables

h	Drop height
$\vec{v}$	Velocity of the package
$\vec{w}$	Velocity of the wind
θ	Angle between package ground velocity ($\vec{v}_g$) and wind velocity ($\vec{w}$).
L	Rope length
T	Threshold error
O	Number of circulations used to determine offset
t	Time

Contents

List of Figures

List of Tables

1
Introduction

This study investigates whether a circular delivery method can enable high-accuracy deliveries using a fixed-wing drone. The research was conducted in collaboration with the SSRS.

1.1 Background

Today, Unmanned Aerial Vehicles (UAVs), or drones as they are commonly called, are used in a wide range of industries such as agriculture, construction and public emergency services. Within these industries, the drones are used for mapping, delivery, photography and filming, just to name a few [1]. In Långedrag Gothenburg the Swedish Sea Rescue Society (SSRS) are developing their own drones, to be used in conjunction with personnel during rescue operations. The main goal of the drones is to, within ten minutes of an alarm, have an on-site view delivered to the rescue crew before departure. This would enable more informed decisions regarding the selection of equipment and boat. With this specific usage in mind, a fix-wing drone was designed (see Fig. 1.1). Later, the question arose as to whether these drones could be used for additional tasks beyond their primary function.

One potential function for the drones would be to deliver packages to recipients at sea. Fixed-wing drones, unlike rotary-wing drones, are unable to hover in place, which makes precise deliveries challenging. In similar situations, a parachute drop is typically used; however, this method can be imprecise, especially in high wind conditions, making it unsuitable for delivering packages to small boats where precision is critical.

One alternative approach would be to use a circular delivery method, where the UAV circles the drop point, with the load extended with a wire. Keeping the package at a lower altitude and velocity than the UAV. Without the aerodynamic effects of the line and the package, centrifugal force would mandate that the package would orbit underneath the circling aircraft. The idea is that this effect could be counteracted with a long enough line, and a well chosen control algorithm for the flight path of the drone.

A preliminary study was performed by A. Käck and O. Wångdahl in 2022, to investigate the possibility of a spiral drone delivery [2]. Their study consisted of setting up a simulation environment, where they could test the circular deliv-

Figure 1.1: The fixed-wing drone used by the SSRS in a combined launcher, display and recharge device. This image was provided by the SSRS

ery method. They could show that it is possible to keep the package to a relatively stable circular path, with a radius smaller than the drone's. To make the drone follow a circular path, they investigated controlling the path using a Proportional–integral–derivative-controller (PID), a Linear quadratic regulator controller (LQR) and a non-linear reference tracking feedback linearization controller (nonlinear). It was shown that the nonlinear controller performed the best for this purpose. While the study used a rigorous model for the drone, rope and package, it used a simple implementation of the wind.

In this study, the previous work will be used as a base and expanded upon. From the previous study, several parts are used with minimal to no alteration. The main parts that are used in full include: The rope model, the nonlinear controller (in accordance with the conclusion of the previous study), the plotting and data saving features. For these features the rope model was only updated to take drag into consideration.

The main goal of this study is to thoroughly investigate the effect of wind and turbulence on the package. Previously, the landing position of the package was estimated before the drop by assuming ideal conditions, such as the absence of wind and air resistance. This study attempts to take these factors into consideration when estimating the landing position. This includes an analytical solution to a system of differential equations that approximates the dynamics of the package. It is also investigated whether the errors stemming from this approximation could be mitigated using a disturbance function. In order to make the simulations as realistic as possible, drag is implemented to allow for the wind to affect the package trajectory.

In addition to improved simulations and landing estimations, the study also includes an updated circular delivery method. This requires a more rigorous methods, as will be explained in Section 3.6, to achieve the optimal conditions for a high accuracy delivery. A fly-by delivery method, incorporating the updated landing position predictor, is also used as a baseline, to evaluate the performance of the circular method.

1.2 Research Questions

During the course of the study, areas of interest include: what factors during the drop affect the error; how can these errors be mitigated, and is it possible to create a disturbance matrix to improve the error. This study aims to answer the following research questions:

- Is it possible to predict where a falling object will land in high wind environments? Can a disturbance function be used to improve the prediction? And how much does turbulence affect the object's landing position?
- How well do the baseline fly-by and the circular delivery method perform? How do these methods compare?

1.3 Limitations and Assumptions

While investigating the research questions, several limitations and assumptions are made, both regarding the environment and the equipment. The first assumption is that the coordinates of the delivery point are known and constant. This corresponds to the recipient boat being stationary and its position being known exactly. It is also assumed that both the drone and the package are equipped with sensors to measure their position and velocity, with the drone additionally equipped with a wind speed sensor. Furthermore, the shape of the package is assumed to be a homogeneous sphere to simplify calculations. It is also assumed that the exact mass and size of the package are known and that the package will be able to withstand the forces exerted on it during the delivery. It is assumed that only gravity and drag forces affect the package. The wind is treated as having high turbulence in order to test the worst-case scenario in that aspect. Lastly, the deliveries are limited to boats without masts in order to allow the drone to fly freely without the line getting tangled in any obstacles.

This study is focused on investigating the concept in form of simulations that circular package delivery with a fixed-wing drone is feasible with an acceptable accuracy defined as within 1 m of the delivery point, which is half the width of the average boat [3]. Factors such as the plausibility of the package surviving the drop are outside of the scope for this study.

1.4 Ethical and Sustainability Aspects

The goal of this study is to develop a precise, autonomous delivery system that eliminates the need for human-to-human interaction. This system could enable faster, more efficient deliveries, particularly in critical situations where time is of the essence. By replacing traditional boat-based deliveries, which rely on fossil fuels, with drone-based solutions powered by electricity, the project also aims to make rescue operations more energy efficient and accurate. The current system requires SSRS volunteers, who must step away from their regular work, to perform deliveries. With a drone based delivery system, the volunteers will only be relied upon during more complex situations.

The primary goal is to deliver life-saving packages to recipients in need. While one could argue that this technology could also be used for harmful purposes, alternative methods already exist that are both faster and more precise for such intents.

2

Theory

Wind is a complex system which makes it difficult to perfectly simulate how an object is affected by it. This can be divided into two parts; first determining the wind's magnitude at a given position and time; and secondly one must determine how a falling object is affected by the generated wind. Additionally, to ensure that the UAV can follow a stable flight path, a reliable control system is also essential. Before addressing these aspects, an explanation of the coordinate systems used throughout this report is provided.

2.1 Coordinate Systems

Four coordinate systems are used for different purposes throughout this report. The first is the *North-East-Down* (NED) coordinate system, which is fixed relative to the cardinal directions: North, East, and a vertical axis pointing downward. The NED frame is commonly used in aerospace applications, as its downward vertical axis aligns with the direction of gravity, offering some advantages over the more conventional *East-North-Up* (ENU) system. Calculations and simulations use the NED coordinate system, while the ENU system is used for three-dimensional spatial plots to provide a more intuitive visual alignment.

The second coordinate system used is a *body-fixed system*, meaning that the coordinate frame is attached to the object and therefore both translates and rotates with it. The axes in this system are defined relative to the object itself: the longitudinal axis, indexed as *long*, points in the direction of motion; the lateral axis, *lat*, runs side to side, such as from wingtip to wingtip in the case of a drone; and the vertical axis, *vert*, is orthogonal to the other two. This vertical axis is not necessarily aligned with the gravity but is instead defined relative to the object's own orientation.

The third coordinate system used is an intermediate version of the other two, that is used for calculations. Like with the NED-system, the Down axis is used as the vertical axis. However, the other two axes are rotated so that one points in the direction parallel to the horizontal movement of the object, here indexed as *par*, and the other axis in the orthogonal direction, indexed as *ort*.

2.2 Wind and Turbulence

One way to simulate the wind is to first determine its steady component and then add turbulence on top of it. The steady component varies with the altitude, a phenomenon that is called *wind shear*. There are several ways to generate random turbulence. In this study the *von Kárman wind turbulence model* is used.

2.2.1 Wind Shear

Knowing the wind at a certain altitude, it is possible to estimate the wind at a different altitude using the *wind profile power law equation*:

$$\frac{w(t)}{w_{\text{ref}}} = \left(\frac{z(t)}{z_{\text{ref}}}\right)^{\alpha}. \tag{2.1}$$

Here w denotes the speed of the wind, z is the altitude above the ground and α is the shear exponent. The subscript *ref* signifies known reference values at a certain altitude. The wind shear exponent depends on the terrain at ground level. An α of 0.11 has been shown to be suitable in most cases for offshore use [4]. The effect of the wind shear with this coefficient can be seen in Figure 2.1.

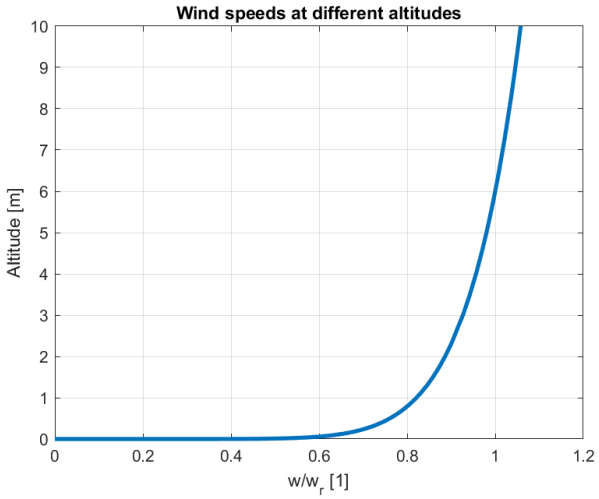

Figure 2.1: Wind speeds at different altitudes according to the *wind profile power law equation* (2.1). A shear constant of 0.11 is used to emulate he conditions at sea. The reference wind speed is w_r at an altitude of 6 m.

2.2.2 Von Kármán Wind Turbulence Model

The von Kárman wind turbulence model is a continuous model that is the preferred turbulence model by the *United States Department of Defense* [5]. The model uses the body-fixed coordinate system to express the velocity components of the turbulence ($w_{\text{long},t}$, $w_{\text{lat},t}$ and $w_{\text{vert},t}$). The turbulence is described with *single-sided spectral densities* for the velocity components. This means that the turbulence is described

in it's frequency domain, using only positive frequencies. This can be done because the values for the positive and negative frequencies are equal, seeing as the signal is real. The spectral densities can be seen in (2.2)-(2.5) [6]:

$$\Phi_{w_{\text{long},t}}(\Omega) = \sigma_{\text{long}}^2 \frac{2L_{\text{long}}}{\pi} \cdot \frac{1}{(1 + (1.339 L_{\text{long}}\Omega)^2)^{5/6}} \tag{2.2}$$

$$\Phi_{w_{\text{lat},t}}(\Omega) = \sigma_{\text{lat}}^2 \frac{2L_{\text{lat}}}{\pi} \cdot \frac{1 + \frac{8}{3}(2.678 L_{\text{lat}}\Omega)^2}{(1 + (2.678 L_{\text{lat}}\Omega)^2)^{11/6}} \tag{2.3}$$

$$\Phi_{w_{\text{vert},t}}(\Omega) = \sigma_{\text{vert}}^2 \frac{2L_{\text{vert}}}{\pi} \cdot \frac{1 + \frac{8}{3}(2.678 L_{\text{vert}}\Omega)^2}{(1 + (2.678 L_{\text{vert}}\Omega)^2)^{11/6}} \tag{2.4}$$

$$L_{\text{long}} = L_{\text{lat}} = \frac{h}{(0.117 + 0.000823h)^{1.2}}, \;\; L_{\text{vert}} = h. \tag{2.5}$$

Ω is the spatial frequency, and σ_i and L_i are turbulence intensity and scale length, respectively, for turbulence component i. The turbulence intensities are determined based on the wind average at 6 m height, and the drop height:

$$\sigma_{\text{vert}} = 0.1 \cdot < |\vec{w}| > \tag{2.6}$$

$$\sigma_{\text{long}} = \sigma_{\text{lat}} = \frac{\sigma_{\text{vert}}}{(0.177 + 0.000823h)^{0.4}}. \tag{2.7}$$

The spectral densities determine the spatial variation in the turbulence stochastically. However, when simulating an object moving with the wind, changes in wind over time must also be accounted for as well as the properties of the moving object, such as the velocity ($V = |\vec{v}_a|$) and its wingspan (b). To do this, it is first necessary to define a new frequency:

$$\omega := V\Omega \tag{2.8}$$

$$\Phi_i(\omega) = \frac{\Phi_i(\Omega)}{V}. \tag{2.9}$$

$$\tag{2.10}$$

Angular turbulence rates (p_i) are also introduced, defined as the variations of the linear turbulence component along the body-fixed axes (x_i):

$$p_{\text{long}} = \frac{\partial w_{\text{vert},t}}{\partial x_{\text{lat}}} \tag{2.11}$$

$$p_{\text{lat}} = -\frac{\partial w_{\text{vert},t}}{\partial x_{\text{long}}} \tag{2.12}$$

$$p_{\text{vert}} = -\frac{\partial w_{\text{lat},t}}{\partial x_{\text{long}}}. \tag{2.13}$$

Based on this, it is possible to determine the power spectral densities for the angular velocity components as following:

$$\Phi_{p_{\text{long}}}(\omega) = \frac{\sigma^2_{\text{vert}}}{2VL_{\text{vert}}} \cdot \frac{0.8\left(\frac{2\pi L_{\text{vert}}}{4b}\right)^{1/3}}{1+\left(\frac{4b\omega}{\pi V}\right)^2} \tag{2.14}$$

$$\Phi_{p_{\text{lat}}}(\omega) = \frac{\pm\left(\frac{\omega}{V}\right)^2}{1+\left(\frac{4b\omega}{\pi V}\right)^2}\Phi_{w_{\text{lat}}}(\omega) \tag{2.15}$$

$$\Phi_{p_{\text{vert}}}(\omega) = \frac{\mp\left(\frac{\omega}{V}\right)^2}{1+\left(\frac{3b\omega}{\pi V}\right)^2}\Phi_{w_{\text{vert}}}(\omega). \tag{2.16}$$

For the purpose of simulating the package under turbulent conditions, the package's diameter (d) is used as a substitute for the wingspan (b).

2.3 Falling Object with Drag

The drag forces acting on an object is directed opposite to its air velocity and is given by the following equation:

$$F_D(t) = -\frac{1}{2}\rho_{\text{air}} C_D A \cdot \vec{v}_a(t)|\vec{v}_a(t)|. \tag{2.17}$$

F_D is the drag force; ρ_{air} is the density of the air, which is the medium through which the object is moving; C_D is the drag coefficient, which depends on the shape of the object; A is the cross section area of the package; lastly, $\vec{v}_a$ is the air velocity of the package, that is, its velocity relative to the wind.

The drag coefficient of an object is not only dependent on the shape of the object, but also its rotation. The only shape that has the same drag coefficient in all directions is the sphere ($C_D = 0.47$), due to its symmetrical nature. With a more irregular shape, the object would spin and change drag coefficient in the direction of relative motion, making it difficult to simulate.

In reality, the object would also acquire some amount of spin, even for a sphere, which in turn would generate a lift force due to the *Magnus effect*. In this study, however, this effect is assumed to be small and is neglected.

2.3.1 An Approximation of the Fall

Considering the effects of drag and gravity, and applying Newton's second law, one can formulate a system of differential equations describing the object's velocity along the different axes. These equations are given by:

$$\frac{dv_{N,a}(t)}{dt} = -\frac{1}{2m}\rho_{\text{air}} C_D A \cdot v_{N,a}(t)\sqrt{v_{N,a}(t)^2 + v_{E,a}(t)^2 + v_{D,a}(t)^2} \tag{2.18}$$

$$\frac{dv_{E,a}(t)}{dt} = -\frac{1}{2m}\rho_{\text{air}} C_D A \cdot v_{E,a}(t)\sqrt{v_{N,a}(t)^2 + v_{E,a}(t)^2 + v_{D,a}(t)^2} \tag{2.19}$$

$$\frac{dv_{D,a}(t)}{dt} = -\frac{1}{2m}\rho_{\text{air}} C_D A \cdot v_{D,a}(t)\sqrt{v_{N,a}(t)^2 + v_{E,a}(t)^2 + v_{D,a}(t)^2} + g. \tag{2.20}$$

The variables ($v_{N,a}$, $v_{E,a}$ and $v_{D,a}$) signify the air velocity of the object, given in a NED coordinate system. This system of differential equation has no analytical solution; however, if one assumes that the wind is constant (no turbulence or wind shear) and neglects the other directional components in each equation, one does get an approximate system with an analytical solution:

$$\frac{dv_{N,a}(t)}{dt} = -\frac{1}{2m}\rho_{\text{air}} C_D A \cdot v_{N,a}(t)|v_{N,a}(t)| \tag{2.21}$$

$$\frac{dv_{E,a}(t)}{dt} = -\frac{1}{2m}\rho_{\text{air}} C_D A \cdot v_{E,a}(t)|v_{E,a}(t)| \tag{2.22}$$

$$\frac{dv_{D,a}(t)}{dt} = -\frac{1}{2m}\rho_{\text{air}} C_D A \cdot v_{D,a}(t)|v_{D,a}(t)| + g. \tag{2.23}$$

This approximation is equivalent to the exact system only when the object has a relative velocity solely along the down-axis. However, when components are added in the north and east directions, it will drift from the solution. The horizontal axes can be rotated such that the horizontal velocity lies entirely along one axis, with no component in the orthogonal direction. This transformation results in a system that more closely approximates the true dynamics than solving the approximate system directly in the NED coordinate frame. In the following sections, the solution to this approximate system will be calculated, first in the vertical, and then in the horizontal plane.

2.3.1.1 Vertical Solution

Along the vertical axis both gravity and drag force are acting on the object, as can be seen in (2.23). Introducing a new variable, v_∞, representing the terminal relative velocity of the object, the differential equation can be simplified:

$$\frac{dv_{D,a}(t)}{dt} = -\frac{g}{v_\infty^2} v_{D,a}(t)|v_{D,a}(t)| + g \tag{2.24}$$

$$v_\infty = \sqrt{\frac{2mg}{\rho_{\text{air}} C_D A}}. \tag{2.25}$$

Depending on the direction of the relative velocity, the drag force will act in different directions. The direction could also change over time, if the object starts off with a relative velocity upwards. However, in the cases of interest in this study,

the object either starts off with positive velocity or a small negative velocity. To be able to solve the differential equation, the drag force is thus assumed to act upwards.

Defining the starting position as the origin and $v_{0,D}$ as the initial vertical velocity, one can solve the differential equation. To get the vertical velocity relative the ground, the vertical wind velocity is added to the vertical airspeed of the object:

$$v_{D,a}(t) = v_\infty \tanh(\frac{g}{v_\infty}(t + C_{1,d})) \tag{2.26}$$

$$v_{D,g}(t) = w_D + v_\infty \tanh(\frac{g}{v_\infty}(t + C_{1,d})) \tag{2.27}$$

$$C_{1,d} = \frac{v_\infty}{g} \tanh^{-1}(\frac{v_{0,D,a}}{v_\infty}). \tag{2.28}$$

From these solutions one can see that the velocity downwards monotonously approaches an airspeed of v_∞ (or a ground speed of $w_D + v_\infty$). To find an equation for how far the object has fallen after any time t, $v_{D,g}$ can be integrated, obtaining the following solutions:

$$s_D(t) = w_D t + \frac{v_\infty^2}{g} \ln(\cosh(\frac{g}{v_\infty}(t + C_{1,d}))) + C_{2,d} \tag{2.29}$$

$$C_{2,d} = -\frac{v_\infty^2}{g} \ln \frac{1}{\sqrt{1 - \frac{(v_{0,D,a})^2}{v_\infty^2}}}. \tag{2.30}$$

It is now possible to estimate the time, t_{ana}, required for the object to fall a given height, by solving equation (2.29), where s_D is set to the desired fall height. This does not have a standard analytical solution, but can be solved with a numerical method (e.g. the Newton-Raphson method). The time t_{ana} can then be used in conjunction with the horizontal solution, to predict where the object will land.

2.3.1.2 Horizontal Solution

As previously mentioned, it is not beneficial to solve for the path in the north and east coordinate frames directly; instead, the path should be rotated so that one axis correspond to the direction of relative motion, and the other axis pointing in the orthogonal direction. Using (2.21), and once again introducing the help variable v_∞, the horizontal component of the system can thus be written:

$$\frac{dv_{\text{par},a}(t)}{dt} = -\frac{g}{v_\infty^2} v_{\text{par},a}(t)|v_{\text{par},a}(t)| \tag{2.31}$$

$$\frac{dv_{\text{ort},a}(t)}{dt} = 0. \tag{2.32}$$

In the orthogonal direction the solutions for velocity, as well as distance traveled, are simple:

$$v_{\text{ort},a}(t) = 0 \tag{2.33}$$
$$v_{\text{ort},g}(t) = w_{\text{ort}} \tag{2.34}$$
$$s_{\text{ort}}(t) = w_{\text{ort}} \cdot t. \tag{2.35}$$

In the parallel direction, the solution is more complex and there are two different solutions depending on the direction of relative motion. However, this can be reduced to one solution by defining the direction of relative velocity as positive:

$$v_{\text{par},a}(t) = \frac{1}{\frac{g}{v_\infty^2}t - C_1} \tag{2.36}$$
$$v_{\text{par},g}(t) = w_{\text{par}} + \frac{1}{\frac{g}{v_\infty^2}t - C_1} \tag{2.37}$$
$$C_1 = -\frac{1}{v_{0,\text{par}}} < 0. \tag{2.38}$$

As done previously, in the other directions, the distance traveled can be found by integrating the ground velocity:

$$s_{\text{par}}(t) = w_{\text{par}}t + \frac{v_\infty^2}{g} ln(\frac{g}{v_\infty^2}t - C_1) + C_2 \tag{2.39}$$
$$C_2 = -\frac{v_\infty^2}{g}\ln(-C_1). \tag{2.40}$$

Using the fall time, t_{ana}, from the vertical solution, the landing position can be estimated using s_{par} and s_{ort}. This position can then be rotated back into the NED coordinate system by defining θ as the angle between the direction of relative horizontal motion and the North axis:

$$\vec{s}_{ana}(t) = \begin{bmatrix} \cos\theta & \sin\theta & 0 \\ -\sin\theta & \cos\theta & 0 \\ 0 & 0 & 1 \end{bmatrix} \begin{bmatrix} s_{\text{par}}\left(t_{\text{ana}}(t)\right) \\ s_{\text{ort}}(t_{ana}(t)) \\ h \end{bmatrix}. \tag{2.41}$$

2.4 Path Controllers

To make the drone follow a stable path, when faced with disturbances such as wind and turbulence, requires the use of a controller. The aim of a controller is to achieve a desired outcome by adjusting the existing behavior. This is achieved with the use of a feedback loop algorithm that takes the current state as an input and gives the necessary changes to the controlling actuators as an output. There are several different controllers. In this study a PID-controller is used for the fly-by algorithm, and a nonlinear controller for the circular delivery. For a more in depth description of how these controllers work, see the previous work by A. Käck and O. Wångdahl [2].

3
Methods

This study consists of three parts. The first involves isolated drops, where a package is dropped from a fixed point, without the involvement of a drone. The goal of these tests is to evaluate the analytical approximation, procured in Section 2.3.1, and research what factors affects the results the most. The second part is a fly-by delivery, where the drone flies straight toward the desired drop point and releases the package when it gets close. The final part is the circular delivery, in which the package is suspended from the drone by a wire while the drone circles the target point. This section will describe the methods used in all three parts.

3.1 Calibration

Throughout the study, certain parameters are kept constant in all simulations. These include some values that may vary in real-world scenarios but are treated as fixed, as their effects are considered outside the scope of this work. The values used for these parameters are listed in Table 3.1.

In some simulations, one or more variables are varied at a time to evaluate their effect on the results. During these simulations, all other variables are kept fixed to default values, which are also listed - alongside the values for the parameters - in Table 3.1.

In the following sections, the reasoning behind the chosen parameter values as well as the default values for the variables are presented.

3.1.1 Parameter Values

When it comes to the values that are treated as constant, the gravitational constant varies in Sweden between $9.815\,\mathrm{m/s^2}$ in the absolute south, and $9.823\,\mathrm{m/s^2}$ in the absolute north of the country [7]. In this study, a value of $9.82\,\mathrm{m/s^2}$ is chosen as that is a close approximation for the whole country. For the air density, a value of $1.225\,\mathrm{kg/m^3}$ is used, as this is the standard sea level density at a temperature of 15 °C [8].

When it comes to the properties of the package, they could very well vary depending on what type of package is delivered. This dependency is outside the scope of this

Table 3.1: The values used for different parameters throughout the study for simulations when it itself is not varied. In the study the effects from varying the parameters in *Variables* section are studied. The variables in the *Parameters* section are, however, treated as known precisely and constant.

Parameters		
Quantity	Notation	**Value**
Gravity [m/s^2]	g	9.82
Air density [kg/m^3]	ρ_{air}	1.225
Package mass [kg]	m	1
Package diameter [m]	d	0.5
Drag constant [1]	C_D	0.47
Shear constant [1]	α	0.11
Shear reference height [m]	z_{ref}	6
Variables		
Quantity	Notation	**Value**
Drop height [m]	h	3
Initial package speed (hor.) [m/s]	$\sqrt{v_{N,g}(0)^2 + v_{E,g}(0)^2}$	6
Initial package speed (vert.) [m/s]	$v_{D,g}(0)$	0
Average wind speed (hor.) [m/s]	$\sqrt{w_N^2 + w_E^2}$	7
Average wind speed (vert.) [m/s]	w_D	0
Angle between velocities [rad]	θ	π

work, and the values used are based on a lightweight defibrillator, serving as an example. The mass is thus chosen to 1 kg. As previously mentioned, the parcel's shape is assumed to be a homogeneous sphere. For a defibrillator to fit, a diameter of 0.5 m is used. Lastly, the drag constant for a sphere is 0.47 [9], [10].

For the constants used in the *wind profile power law equation* (2.1), a shear constant of 0.11 is used, since this is the recommended value for offshore calculations, as previously mentioned. For the reference height, 6 m is used, as that is the standard used by the MATLAB toolboxes used for the code. This means that whenever a wind velocity is given, it refers to wind velocity at a height of 6 meter, not at the altitude of the drone or the package.

3.1.2 Default Variable Values

For the drop height, a value of 3 m is used as default. This is because, intuitively, the accuracy of the drop decreases with increasing height, as the package is exposed to wind and turbulence for a longer duration before landing. However, releasing the package from a height lower than 3 m could result in the drone colliding with the recipients on the boat.

The remaining default values are primarily used in the isolated drop tests. One of the primary goals of these drops is to determine the expected accuracy with the

circular delivery for different conditions. To determine suitable default values for the package's velocity in the horizontal and vertical directions, respectively, early simulations were done. These showed horizontal velocities close to 6 m/s and vertical velocities close to 0 m/s.

For the average horizontal wind speeds, data from the weather station Vinga A - located in the archipelago outside of Gothenburg - was used. Between the dates of the first of January 2015 and the 31st of December 2024 the average recorded was a speed of 7 m/s at a height of 18 m [11]. Adjusting this with shear for the used reference height of 6 m, this corresponds to a wind speed of about 6.2 m/s. Since the disturbance function is later generated using integer wind speeds, and to ensure the default value represents conditions that is slightly harsher than average, a wind speed of 7 m/s is chosen. The average vertical wind is assumed to be negligible, and a value of 0 is used as default.

For the angle between the horizontal velocities of the wind and the package, a default of π rad is used. The reason for this being that it is expected to be easier to control the drop when the velocities are parallel, that is either perfectly in the same direction or in opposite directions. π is chosen over 0 as it is desirable if the package has a low velocity at arrival. Releasing the package headwind would, at least initially, cause the wind to slow the package down.

3.2 Isolated Drops

The purpose of the isolated drops can be divided into three parts. The first is to determine how good an approximation of the fall the estimation from Section 2.3.1 is, and what variables affect the error the most. The second goal is to determine whether the error can be mitigated by pre-running simulations for some combinations of parameters, and using the recorded errors between the estimation and actual landing as an offset for future runs with similar values. The final objective is to analyze how much turbulence contributes to the error, and under which conditions this effect is minimized.

The package is simulated using the differential equations (2.18)-(2.20), with a time step of 0.01 s. In all simulations, wind shear is used, but depending on the simulation the turbulence can either be enabled or disabled.

3.3 Disturbance Function

The aim of the disturbance function is to use stored values from previous simulations to be able to mitigate the fact that the analytical estimation for the drop is not the solution to the true system of differential equations. For all or some of the six variables studied in this report, different values within the relevant range are chosen. Then simulations are run without turbulence for each combination of these chosen variables, while the remaining variables are set to their defaults. For

each combination of values, the difference between the simulated landing position and the prediction from the analytical estimation is simulated. These are stored in two different tensors, where each variable that is chosen to vary makes up one dimension. The two tensors contain errors in the directions parallel and orthogonal to the package's initial horizontal velocity, respectively.

When predicting the errors for a new set of values, the variables varied when generating the disturbance function are used as an input. Based on their values, the corresponding indices of the input vector within the tensor are calculated as if the tensor were continuous. For example, if the input value for the horizontal wind speed is right in between the values of the second and third value used to create the tensor, it is given an index of 2.5 for this variable.

Based on these calculated indices, a predicted value is calculated by linearizing around the closest values in the tensor. This is done with a multivariate Taylor expansion using discrete derivatives:

$$\vec{I} = [I_1, I_2, ..., I_n] \tag{3.1}$$

$$\vec{F} = [\lfloor I_1 \rfloor, \lfloor I_2 \rfloor, ..., \lfloor I_n \rfloor] \tag{3.2}$$

$$D_{\text{par},i} = E_{\text{par}}(F_1, \ldots, F_{i-1}, F_i + 1, F_{i+1}, \ldots, F_n) - E_{\text{par}}(\vec{F}) \tag{3.3}$$

$$D_{\text{ort},i} = E_{\text{ort}}(F_1, \ldots, F_{i-1}, F_i + 1, F_{i+1}, \ldots, F_n) - E_{\text{ort}}(\vec{F}) \tag{3.4}$$

$$P_{\text{par}}(\vec{I}) = E_{\text{par}}(\vec{F}) + \sum_{i=1}^{n} (I_i - F_i) \cdot D_{\text{par},i} \tag{3.5}$$

$$P_{\text{ort}}(\vec{I}) = E_{\text{ort}}(\vec{F}) + \sum_{i=1}^{n} (I_i - F_i) \cdot D_{\text{ort},i}. \tag{3.6}$$

Here $\vec{I}$ is a vector containing the continuous indices for the input; $\vec{F}$ is the floor of each index; E_{par} and E_{ort} are the tensors of stored errors from previous simulations in the directions parallel and orthogonal to the package's velocity, respectively; $D_{\text{par},i}$ and $D_{\text{ort},i}$ are the discrete partial derivatives with respect to variable i; and P_{par} and P_{ort} are the predicted errors in both directions. If the function receives an input value outside the range used to generate the matrix, it assumes the error varies linearly from the nearest value within the range.

The landing prediction can then be updated with a distance $\vec{s}_{dist}$ that can be given in the NED coordinates by rotating the results from the disturbance function $-\theta$ rad, where θ denotes the angle between the horizontal component of the package's velocity and the North axis:

$$\vec{s}_{dist} = \begin{bmatrix} \cos\theta & \sin\theta & 0 \\ -\sin\theta & \cos\theta & 0 \\ 0 & 0 & 1 \end{bmatrix} \begin{bmatrix} P_{\text{par}} \\ P_{\text{ort}} \\ 0 \end{bmatrix}. \tag{3.7}$$

The time it takes to generate the disturbance function, as well as the data needed to

store its information grows quickly with the number of variables and variable values used in its generation. Both the time and the storage space is proportional to:

$$\prod_{i=1} n_i. \tag{3.8}$$

The index i represents the variables in the function, and n_i is the number of values for variable i that was used to generate the function. The generation time and data thus grows exponentially with the number of variables, and polynomially with n (assuming that the same n for each variable).

3.4 Release Mechanism

For both the fly-by delivery and the circular delivery, an algorithm to determine when to release the package is necessary. In every time step, a calculation is performed to estimate where the package would land were it to be released during the current time step. This is done using the analytical estimation and the disturbance function. The foundation for the mechanism is to release the package when the distance between the estimated landing point and the target point is smaller than a threshold error (T).

If only this method is used, the UAV would always release the package as soon as it gets within the threshold error, even if the error would decrease further were the package to be released later. To counter this, an additional criterion is introduced: the current expected error must be greater than the previous expected error. This added criterion introduces an error: the package will consistently be released one time step after the optimal one. One solution would be to instead calculate where the package to be released the next time step. This requires assuming that the package maintains a constant velocity until that time. The expected outcome of this addition is the package being released one time step earlier, unless there is a sudden change in the velocity of the package. In total, the package is released when the following criteria are met:

$$\vec{e}(t) \equiv \vec{p}(t) + \Delta t \cdot \vec{v}_g(t) + \vec{s}_{\text{ana}}(t) + \vec{s}_{\text{dist}}(t) - \vec{d} \tag{3.9}$$

$$|\vec{e}(t)| < T \tag{3.10}$$

$$|\vec{e}(t)| > |\vec{e}(t - \Delta t). \tag{3.11}$$

$\vec{e}(t)$ is the estimated landing error calculated at time t, representing the predicted error if the package were to be released at time $t + \Delta t$; $\vec{p}$ is the current position of the package; $\vec{v}_g$ is the current ground speed of the package; $\vec{s}_{\text{ana}}$ is how far away the package should land according to the analytical estimation (2.41); $\vec{s}_{dist}$ is the correction from the disturbance function (3.7); $\vec{d}$ is the desired landing point, and T is threshold error.

3.5 Fly-by Drops

A naive idea for a delivery method using fixed-wing drones would be flying straight toward the desired drop point and release the package according to the release mechanism from Section 3.4. Simulations with this fly-by approach are done as a baseline to compare the circular delivery method to.

The drone either approaches the drop point in the direction of the wind or directly against it. To make the drone follow a straight path with a constant airspeed, a PID controller is used. The controller can handle wind speeds up to:

$$|\vec{w}_{max}| = -\frac{1}{2} + \sqrt{|\vec{v}_a(t)|^2 + \frac{1}{4}}. \tag{3.12}$$

The controller used in MATLAB crashes when this value is surpassed, making it necessary to cap the norm of the wind to this value. To be able to handle the range of wind velocities from $-15\,\mathrm{m/s}$ to $15\,\mathrm{m/s}$, without regularly exceeding the maximum wind due to turbulence, an airspeed of $20\,\mathrm{m/s}$ is chosen as the target for the drone.

3.6 Circular Delivery Method

To explain the methodology surrounding the circular delivery method some simulation images will be used (see Fig. 3.1 for an example). These images are shown using the ENU (East-North-Up) coordinate system, which matches how the directions are usually perceived. The drone is depicted as a small fixed-wing drone model in the three-dimensional plot and a red triangle in the top-down plot. The path of the drone is shown as a dark red line. Similarly, the package is shown as a blue square and its path is shown as a blue line. The light blue line in the three-dimensional plot represents the rope towing the package. The orange star is the target point for the delivery. Lastly, the green dot represents the currently calculated drop point for the package, if it were to be released at the current time step, and the green line shows all previously calculated drop points. Lastly, the smaller red, blue and green lines emitting from the drone shows the orientation of the drone with the green line showing left, the red forward and the blue down.

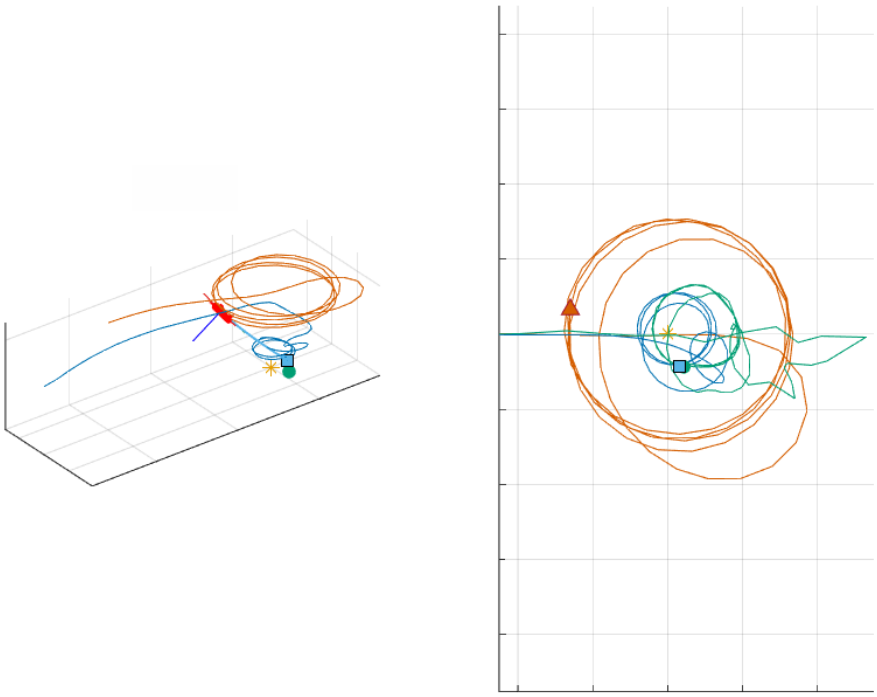

Figure 3.1: The resulting pathway for the drone using the circular pathing after 36.5 s of simulation with no wind. On the left, a three-dimensional view, on the right a top-down view.

3.6.1 Controller and Field Experience

In study [2] the nonlinear controller was deemed the best for the purpose of circular delivery [2]. However, during testing with the more rigorous implementation of wind, it became apparent that the circular path kept by the nonlinear controller quickly became erratic and unstable when subjected to wind larger than minor turbulence. In Fig. 3.2 the drone can be seen attempting to circle the target point in 8 m/s wind.

The SSRS already uses a controller that allows for a drone to circle around a point with high precision and stability despite wind. However, this controller is currently not compatible with MATLAB, and the code used in this study. The decision was therefore made to use the nonlinear controller from [2] to emulate the results from the already existing controller by applying low turbulence to the drone.

To provide real-world data for comparison, the log from a test flight made by the SSRS on 3 December 2024 was used (see Figs. 3.3 and 3.4). During this flight, the drone was instructed to circle around a point for two laps, then increase its target airspeed by 1 m/s, slightly shift the center point and then complete two additional laps. This procedure was repeated for the drone airspeeds of 12 to 30 m/s. From this log, the two laps flown at a speed of 15 m/s were extracted along with the corresponding wind velocities. In Fig. 3.3 the flight path can be seen to closely follow each other for the two laps despite the ca 8 m/s wind shown in Fig. 3.4.

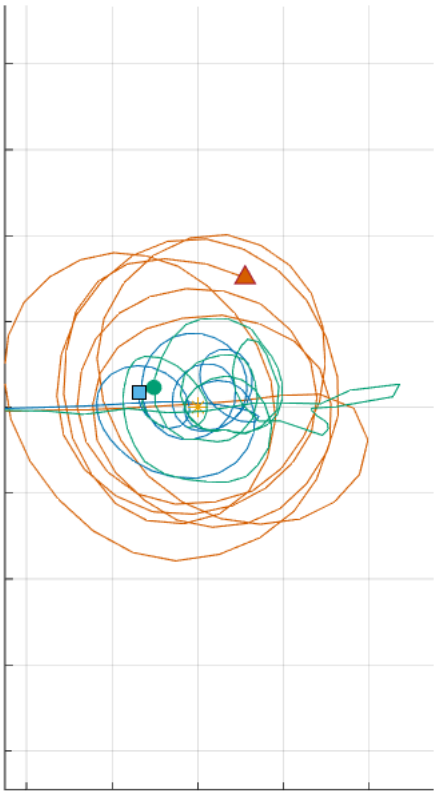

Figure 3.2: The path of the drone, package and predicted landing spot while the nonlinear controller attempts to circle the target point while the drone is affected by 8 m/s turbulent wind.

Figure 3.3: The flightpath of a drone during testing at Långedrag during 3 December 2024; the data was provided by the SSRS.

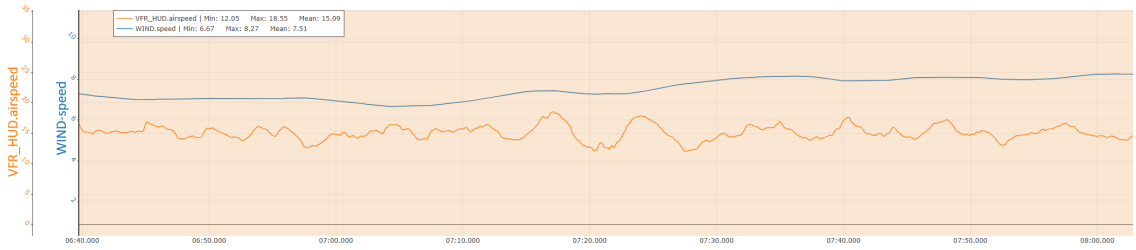

Figure 3.4: Wind speed (blue) and drone airspeed (orange) during the flight seen in Fig. 3.3. The wind fluctuates at around 7-8 m/s. And the drone kept an airspeed at around 15 m/s.

Using the path from this test flight, the wind affecting the drone in the simulations was, through testing, limited to the turbulence of the wind capped at 0.3 m/s. The resulting circular path of the drone, controlled by the nonlinear controller can be seen in Fig. 3.5. In this figure, the simulated drone path resembles the recorded drone path from the real-world test, seen in Fig. 3.3 as was the goal.

3.6.2 Release Mechanism Constraints

Due to the complex nature of the circular delivery method, further constraints are needed for the release mechanism, explained in Section 3.4, in order to maximize the accuracy of the drop. Firstly, the height at which the package is dropped greatly affects the error as will be presented in Section 4.1.1. Therefore, the package must not be dropped if its height exceeds 5 m. Initial simulations showed that increased vertical speed of the package at drop also greatly increases the error. Therefore, if the vertical velocity is greater than 0.2 m/s the package is not dropped. However, in later simulations, see Section 4.1.1, the error was smaller than initially believed, but the constraint was kept.

3.6.3 Rope and Package Model

A model of the rope connecting the package to the drone was created using 20 segments. The first segment is attached to the drone, and the last to the package. Each segment is then treated as a point mass halfway between the two ends of the segment, with velocity averaged from both ends. All pieces of the rope are affected by both gravity and drag, while some are also affected by the pulling forces from the drone in a forward direction, and the weight of the package in a downward direction. The rope was defined as a 3 mm diameter, density of 7 g/m and made of polyester with a Young modulus of 1 GPa.

The velocities of the rope segments is calculated through several steps. The velocity of each rope segment is updated based on the speed of which the drone is pulling the rope. Drag is then applied to the average velocity of the two ends of each rope segment. Then a generalized coordinate system describing the rotation of the cable

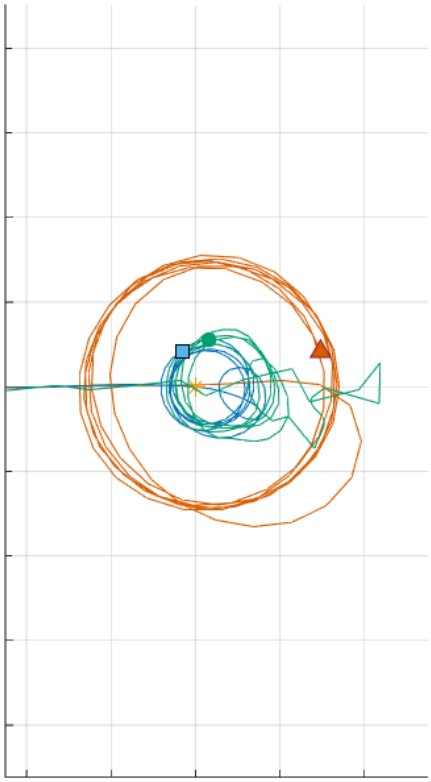

Figure 3.5: The path of the drone, package and predicted landing spot while the nonlinear controller attempts to circle around the target point while the drone is affected by a maximum of 0.3 m/s wind turbulence.

is created and the velocity is split up into parallel and normal directions based on this coordinate system. The velocity is used to calculate the mach number of flow in each direction, this is used to calculate cable skin-friction drag coefficient and the normal drag coefficient, which in turn is used to calculate the drag coefficient and the lift coefficient. These coefficients are used to calculate the drag and lift forces applied to the end of each rope segment. The force on each point mass of the rope is then calculated by taking the average of the two segment ends [12].

The next step is to apply a newton law model to apply the force of the rope pulling itself using the Young modulus. This force combined with the lift and drag force calculated previously, as well as the gravitational force is used to calculate the acceleration of each rope segment which gives the final velocity of the rope [12].

The velocity of the package is calculated simultaneously as the rope. The endpoint of the rope is treated as the package by changing it's weight to that of the package. The drag is then calculated separately from the rest of the rope [12].

3.6.4 Helical Vertical Descent

Because the error increases with the drop height, the release altitude must be kept low. However, with wind, and more importantly turbulence, the package does not hold a constant height relative the drone. Therefore, a dynamic height regulator is required to keep the package low enough to minimize error, while ensuring it does not risk landing in the water.

The base of the function is a helical vertical descent where the drone slowly descends depending on the package's height. This function requires a height-span in which the package is to be kept. The span is defined as between 2.5 m and3.5 m to keep the package at around 3 m. The first step of the function is to wait until the drone has arrived an circling the delivery position. Then, each second, the function logs the lowest package position and if the lowest height is under our minimum height, the drone will increase it's height by 0.1 m. If the the package is higher than the defined maximum height the drone will decrease it's height by $0.1 \cdot difference/4$ if $difference$ is larger than 4 m, otherwise by 0.1 m. Here $difference$ denotes the distance from the current height to the desired maximum height. The one second sample size and the small changes are to allow the drone time to react and descend or ascend to the new height. The resulting descent can be seen in Fig. 3.6 where the drone drops from a height of approximately 40 m to a height of around 25 m. This also allows the package to drop from a height of about 20 m to a height of about 5 m.

Currently the helical vertical descent function works in most cases, but occasionally fails and the package reaches a negative height in the simulations. However, this has no effect on the resulting error from the drops, due to the height from which the packages are being dropped is located close to the desired range.

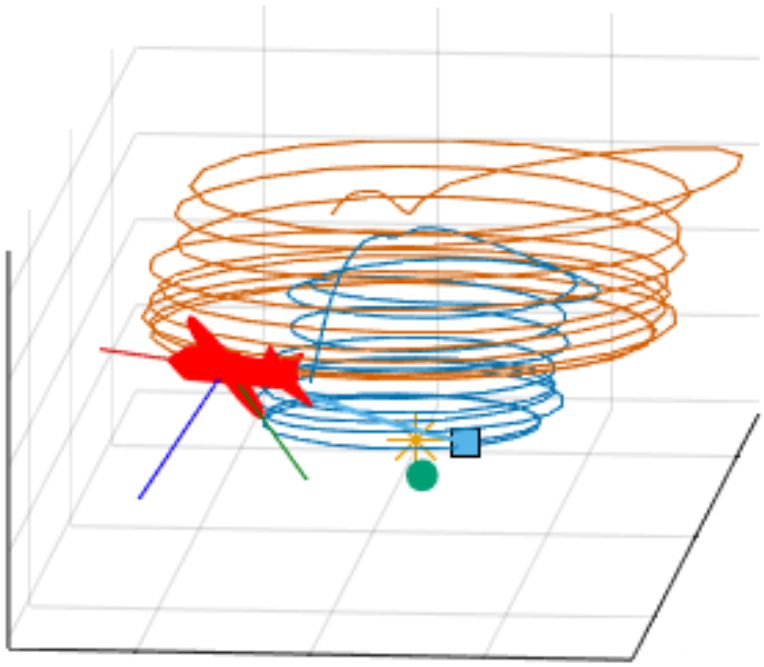

Figure 3.6: A helical vertical descent that gradually decreases the circling height of the drone in order for the package to reach a more acceptable height from which to be dropped.

3.6.5 Offset Function

Another function needed for the circular delivery is an offset regulator. Unlike in the fly-by delivery, where the course of the drone could simply be moved to counteract the wind, the circular delivery method requires a more robust method. For the definition of this function we define that the drone approaches the site in an easterly direction (right in the figures) directly against the wind to simplify the function. However, the function could easily be remedied to account for when the drone approaches from other directions.

When the drone arrives at the site, it begins to circle the delivery point in a clockwise direction with the delivery point in the center (this is arbitrary and could easily be changed to counterclockwise). The function waits for the drone to complete a full turn around the delivery point and for it to reach an acceptable height (defined as five meters, two meters above the wanted drop height) to allow for the drone to stabilize in it's circular trajectory and the package altitude. The function will then log the northernmost point of the circular trajectory created by the drop point estimation function. After the drone has done a defined number of passes and as many northerly distances have been logged, the function calculates the average distance from the delivery point that the drop point circles, and moves the center that the drone circles that same distance to the south. This will ensure that the calculated drop point of the package will pass closely to the delivery point with regardless of drone velocity and wind conditions. The drone moves in a southerly direction to make sure that the package is dropped against the wind. and for tests where the

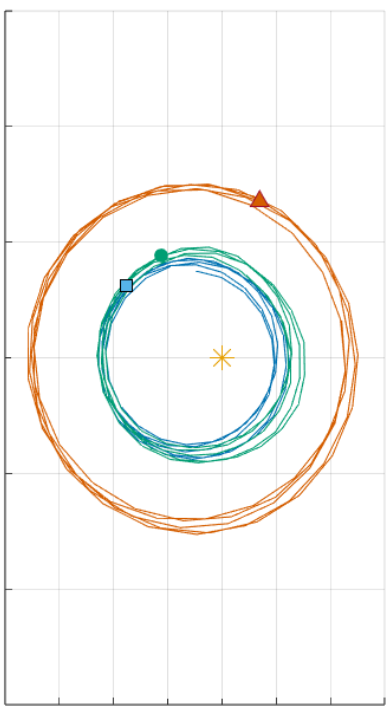

(a) The drone, package and drop point path before the offset function moves the center point which the drone circles.

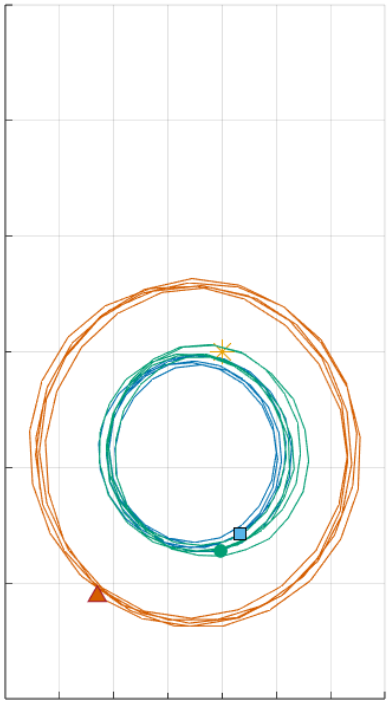

(b) The drone, package and drop point path after the offset function moves the center point which the drone circles.

Figure 3.7: The path of the drone, package and predicted landing position during the offset function execution.

package is dropped with the wind, the drone will move in a northerly direction.

In Fig. 3.7, the path of the drone is shown before (Fig. 3.7a) and after (Fig. 3.7b) the offset function has been executed. In the before image it is clear that the drop point path (green line) will never cross close enough to the target point (yellow star). On the contrary, in the after image (Fig. 3.7b) it is clear that the drop point path is close to the target point on most passes. This should allow for a acceptably close drop point to be found if the drone is allowed to circle for a long enough time.

A manual offset of 5 m to the west is also applied. During early simulations it was found that the package is often dropped with an initial velocity angled at almost $pi/4$ rad compared to the wind. With the manual offset this is changed to be much closer to 0 degrees. The offset of 5 m has, during simulations, not appeared to significantly change with wind speed or the speed of the drone or package.

4
Results and Discussion

First, the results for the isolated falls are shown and discussed to generate an apt disturbance function, and to determine how best to perform the fly-by and circular deliveries. Then the results for these delivery methods are presented.

4.1 Isolated Falls

For the isolated falls, simulations are first done without turbulence to evaluate the accuracy of the analytical approximation. Then a disturbance function is generated to determine if it can mitigate these errors. Thereafter turbulence is added to the wind to see how large an impact turbulence has.

4.1.1 Evaluate Approximation

To begin, isolated drops were made without turbulence or any disturbance function, to determine the precision of the analytical approximation. The results when varying one variable at a time can be seen in Fig. 4.1. Most of the time, the analytical solution gets within a couple of centimeters from the actual solution; however, it is still important to minimize the errors from each source as much as possible. It is also important to note that these values were obtained by varying only one variable at a time from the default values. Even larger errors can be observed when changing multiple variables simultaneously, though they are expected to be in the same order of magnitude.

One way to minimize the errors from the estimation is to create a disturbance function as described in Section 3.3. Ideally one would create a disturbance function based on all six variables, and with a high number of values for each. Seeing as the data and generation time scales quickly with the number of variables and values, that might not be realistic, and it is important to determine what variables and values are most important. Another way to limit the errors is to make sure that the package drop occurs when the variable values are as favorable as possible.

4.1.1.1 Implications for the Fly-by Delivery

For the fly-by delivery, the drop height and the package's vertical velocity is kept low by the drone's control system. The angle between the velocities could also be kept close to either 0 or π by selecting the direction of approach to the drop point.

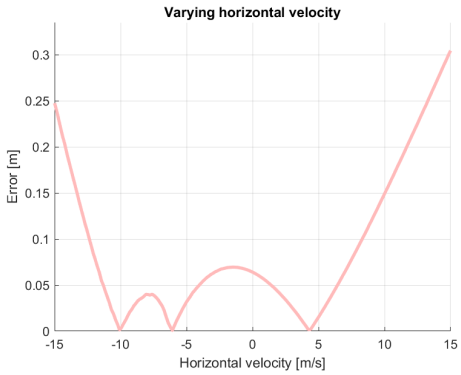

(a) Varying the package's horizontal velocity

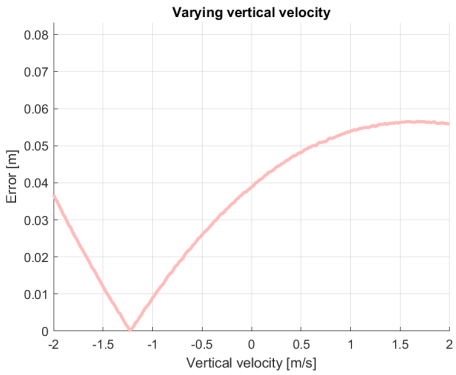

(b) Varying the package's vertical velocity

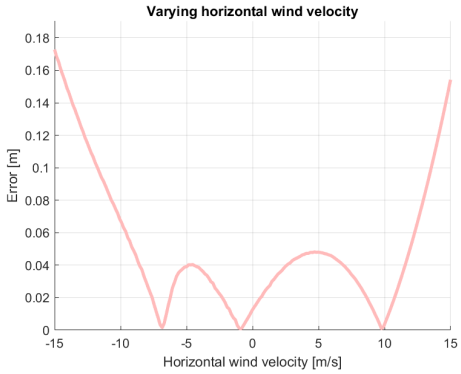

(c) Varying the wind's horizontal velocity

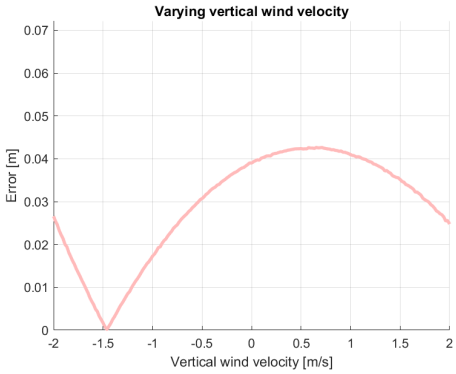

(d) Varying the wind's vertical velocity

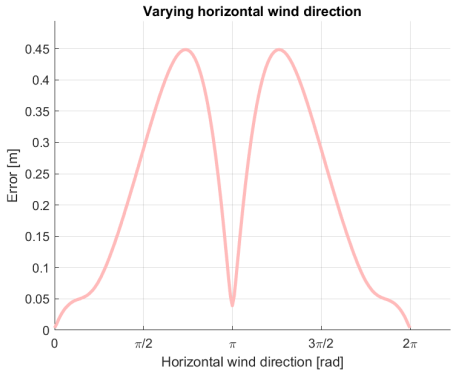

(e) Varying the angle between the velocities

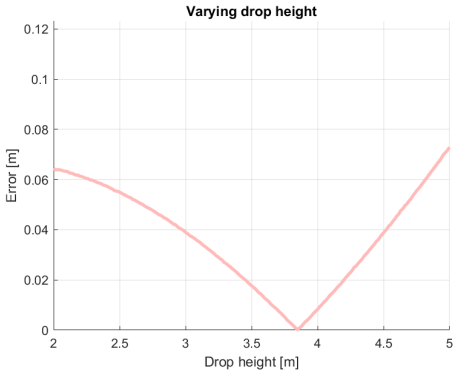

(f) Varying the package's initial height

Figure 4.1: Simulations for how accurate the analytical estimation is when varying one variable at a time for isolated drops. The parameters not varied are assigned the default values listed in Table 3.1. Note that due to the default angle of π rad, either a negative package or wind velocity represents a tailwind release. Also note that the positive vertical direction is downward.

Of note is that the minimum at π appears more volatile than the one at 0, so it might be a bit more stable to release the package tailwind. However, there are other factors to consider when determining the drop direction. For example, it is important to assess the impact of turbulence in both directions. Additionally, the landing velocity of the package should be taken into account, as large velocities might harm either the package or the recipient.

Thus the remaining variables are the wind velocities in both directions as well as the package's horizontal velocity. The wind velocities can never be controlled regardless of algorithm. When it comes to the package's velocity, its initial velocity is the same as the drone velocity at release. Since the drone must fly with a higher airspeed than the wind (as explained by (3.12)), the initial horizontal ground velocity is larger for tailwind drops than headwind drops. This results in reduced accuracy from the analytical approximation.

For a disturbance function it would be necessary to use multiple values for the horizontal package velocity, especially if tailwind releases are done. The horizontal wind velocity is also important as it cannot be controlled and it causes significant errors in the estimation. The angle between the velocities is kept close to either 0 rad or π rad by the drone's control system, and it is thus not as important as it will later be for the circular delivery. The minima at these angles, especially at π rad is, however, volatile, which could be improved by using angles close to the minima in the disturbance function. The errors resulting from the remaining variables are comparably small.

4.1.1.2 Implications for the Circular Delivery

For the circular delivery, one can draw similar conclusions as for the fly-by delivery. However, it is harder to control both the angle of the velocities as well as the drop height. By design, the angle is constantly changing, and even if the drone retains a stable altitude, the package might not. The deviations in the altitude is, however, not expected to be large once the drone has settled into a stable circling flight path.

One can try to release the package as close to headwind or tailwind as possible by selecting the circling point such that the optimal release timing occurs when the package is moving parallel to the wind. This would be harder to control than in the fly-by case, making the volatility of the minima for the angle more apparent.

Another difference from the fly-by drop is that the horizontal speed of the package is expected to be kept relatively close to 6 m/s regardless of drop direction. It is thus unlikely that the drop would occur in the ranges with larger errors.

For a disturbance function, both the horizontal wind velocity and the angle between the velocities are important factors to incorporate. The velocity of the package might also be relevant enough, as the derivatives of the errors are large close to both -6 m/s and 6 m/s. For the remaining variables it would likely be sufficient to only use one set of values for the disturbance function.

4.1.2 Implementing a Disturbance Function

Based on the results from the previous section, a disturbance function was generated using the horizontal velocities of the package and the wind, as well as the angle between them. For the horizontal package velocity, all integer values in the range [0, 15] were used, and for the horizontal wind velocity, integer values in the range [−15, 15] were used. For the angle, 10 values uniformly distributed in the range [0, $\pi/4$] were used. Using symmetry and the fact that negative values for the horizontal wind velocity were used, this means that it can handle angles in the ranges [$-\pi/4$, $\pi/4$] as well as [$3\pi/4$, $5\pi/4$]. For the other variables only the default values were used, to make the function quicker to generate. This disturbance function covers the relevant ranges for both delivery methods, except tailwind releases with the fly-by delivery. This case will be studied more in Section 4.1.5. The results from using this disturbance function can be seen in Fig. 4.2.

4.1.2.1 Varying Variable not in Disturbance Function

When varying one of the variables for which only the default value was used during the generation of the disturbance function (i.e., the drop height or any of the vertical velocities), the disturbance function always predicts the same error from the analytical estimation. This is because the output from the disturbance function depends only on the variables for which multiple values were used during its generation. The error it predicts corresponds to the simulation using default values for all variables, approximately 4 cm, as seen for the default values in any subplot. However, if the same graphs were generated with one of the variables in the disturbance function set to a non-default value, the predicted correction would differ. This is illustrated in Fig. 4.3, where both the drop height and the package's vertical velocity are varied.

For other values in these graphs, the only error in the disturbance function it is basing itself upon, is still the one with the default values. This is a result of these variables not being an input of the disturbance function, making the output independent of their values. Thus the function offsets all values by the same amount, regardless of the simulated error. For values where the analytical error vector is pointing in the same direction as for the default values and at least half as large as for the default value, the accuracy is better. When that is not the case, as for example for initial heights larger than approximately 3.5 m, the ultimate error is larger. So, the disturbance function improves the results, as long as the deviations around the default values are small.

If the deviation would turn out not to be small enough, one solution would be to use more than one value for these variables to generate the disturbance function. If this is not desirable, another alternative is to generate the function using another value for the parameters, around which the maximum errors are smaller in the relevant range. This would result in non-zero errors at the default values.

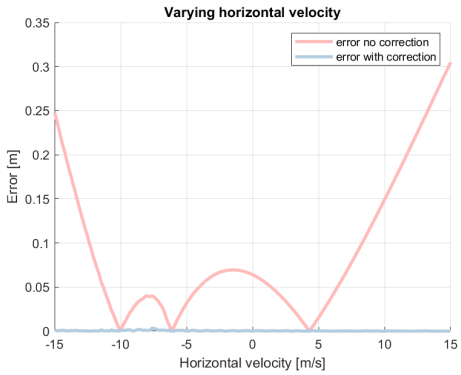

(a) Varying the package's horizontal velocity

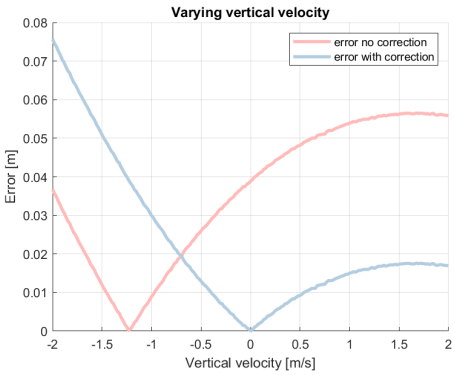

(b) Varying the package's vertical velocity

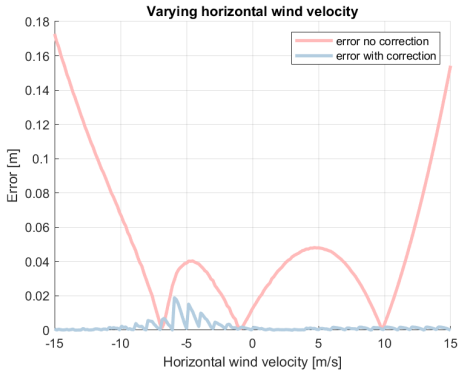

(c) Varying the wind's horizontal velocity

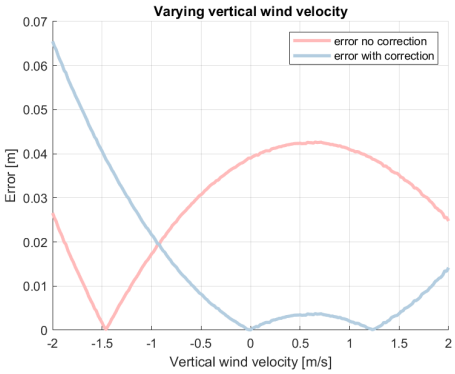

(d) Varying the wind's vertical velocity

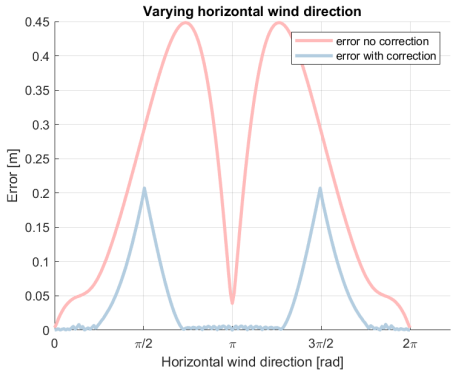

(e) Varying the angle between the velocities

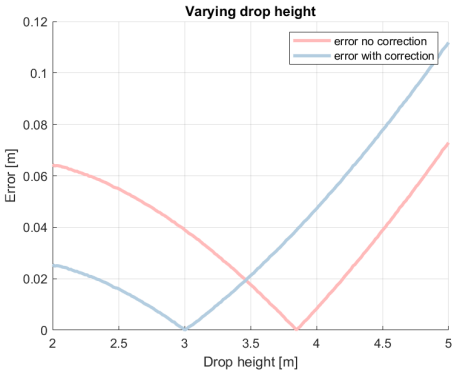

(f) Varying the package's initial height

Figure 4.2: Simulations comparing the errors from the analytical solution, for isolated drops, with and without the addition of a disturbance function. The parameters not varied are assigned to the values listed in Table 3.1. Note that due to the default angle of π rad, either a negative package or wind velocity represents a tailwind release. Also note that the positive vertical direction is downward.

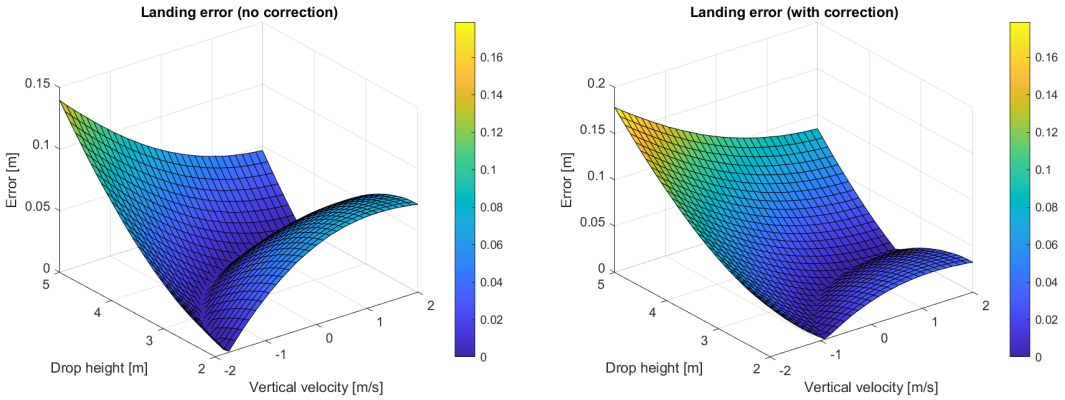

(a) Disturbance function not used **(b)** Disturbance function used

Figure 4.3: Simulations showing the errors resulting from the analytical estimation, with and without the disturbance function applied, when varying both the height from which the package is dropped as well as the package's initial vertical velocity.

4.1.2.2 Varying Variable in Disturbance Function

Varying any of the variables in the disturbance function (i.e. any of the horizontal velocities or the angle in between them), it is apparent that the disturbance function does lower the errors significantly. When varying the package's horizontal velocity, the error is close to nonexistent for all values. Keep in mind that this would not be fully true when any of the parameters not in the disturbance function deviates from the defaults, as can be seen in Fig. 4.4, where both the package's velocity and the drop height are varied.

In the simulation varying the horizontal wind speed, one can see a few spikes around $-5\,\mathrm{m/s}$ after applying the disturbance function. These have minima at the integer values, as these have been used when generating the disturbance function. Between the integers values the disturbance function assumes the error to be linear; however, observing the corresponding graph without the correction, it is far from linear in this region. The larger the second derivative of the error without correction, the larger these spikes will be. However, compared to the error without any correction, the errors at these spikes are relatively small. One problem that could potentially arise from them is when they are comparable in size to the distance the package moves in one time step, as they could then cause the release mechanism to erroneously estimate a larger error than the previous time and release the package prematurely.

In an attempt to estimate how likely these spikes are to impact the release mechanism at the estimated package speed at release of $6\,\mathrm{m/s}$, one can study the error after applying the disturbance function, when varying both the speed and the direction of the wind (see Fig. 4.5). One can see that the maximum size of any spike for the fixed package speed is below $2\,\mathrm{cm}$, and occurs for a combination of a high wind speed and a large angle. For more moderate situations, the size of the spikes stays below $1\,\mathrm{cm}$. As the simulations are run with a time step of $0.01\,\mathrm{s}$, the package is expected to move $6\,\mathrm{cm}$ each time step. This is multiple times larger than the size of

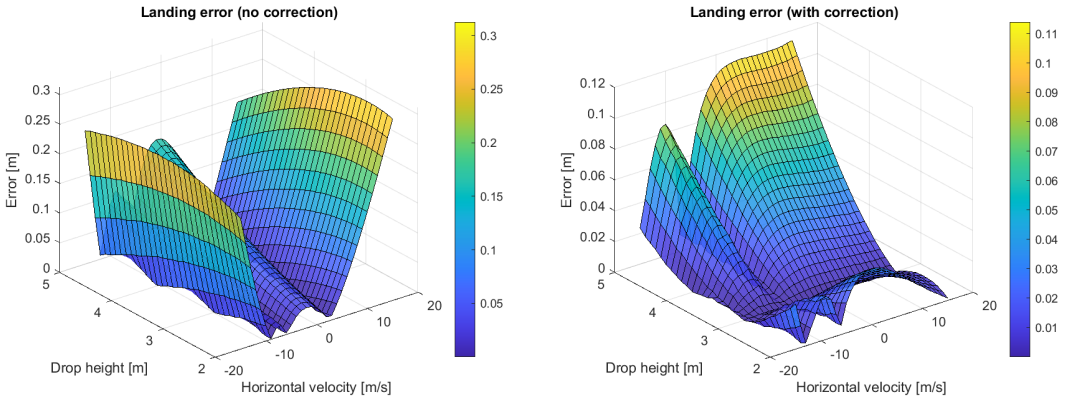

(a) Disturbance function not used **(b)** Disturbance function used

Figure 4.4: Simulations showing the error from the analytical estimation, with and without the disturbance function applied, when varying both the height from which the package is dropped as well as the package's initial horizontal velocity. Note that the scales for the color bars are different.

the spikes, which makes it unlikely that a spike could, on its own, cause the release mechanism to release the package.

There are at least two ways one could go about decreasing the size of the spikes, if they were to be a problem. One simple solution would be to use more data points in the disturbance function, which would decrease the size of the spikes. As shown in Section 3.3 this has some drawbacks when it comes to the time it takes to generate the function and the data needed to store it. Another potential method would be to assume the error to follow a second order equation between values rather than being linear, by extending the Taylor-expansion in the disturbance function to the second order.

In Fig. 4.2e one can see how the disturbance function works outside the range of used angles. Within the active area of the disturbance function (that is within $\pi/4$ of either 0 or π) it works as intended. Outside those ranges, there are spikes similar to the ones observed for the horizontal wind velocity. These ones though are larger, in large part due to the fact that the distances to the values in the disturbance function get larger. As the graph for the errors is monotonic outside of the active range, one could expect the errors to be decreased by the fact that the disturbance function assumes continued linearity. The reason why this is not observed might be due to the fact that even though the size of the errors appears to follow a close to linear relation, the direction of the error changes with the direction of the wind, which the disturbance function does not consider.

If a larger range of angles had been relevant to the delivery algorithms it would be important to include the full range of angles in the disturbance function. The largest spikes are currently roughly 2 dm even with all other values at their defaults. This would be a major source of error if these angles were of interest.

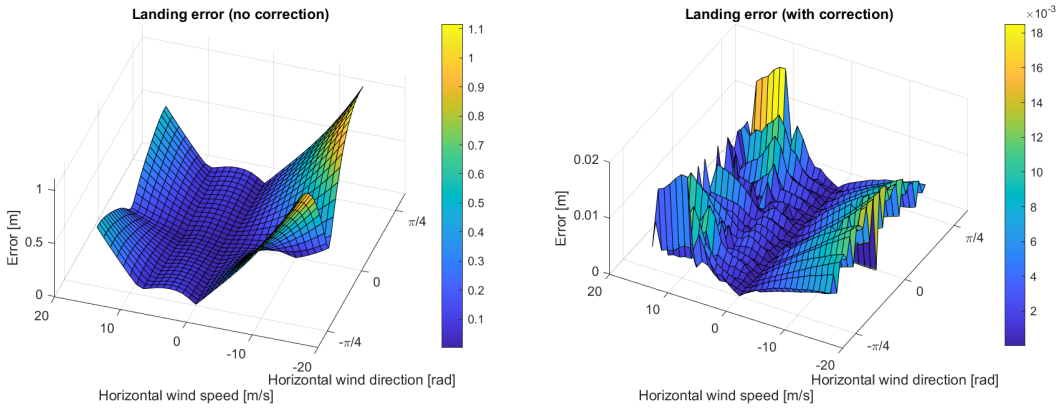

(a) Disturbance function not used **(b)** Disturbance function used

Figure 4.5: Simulations showing the error from the analytical estimation, with and without the disturbance function applied, when varying both direction and average horizontal speed of the wind. Note that the scales for the color bars are different.

4.1.3 Isolated Falls With Turbulence

With turbulence added to the simulations, the landing position varies between runs, even with identical inputs. This makes it important to repeat each simulation multiple times to get statistically meaningful results. In Fig. 4.6, a scatterplot is shown for 1000 simulations released in a strong headwind, both with and without the disturbance function applied. The same simulations also include a *cumulative distribution function* (CDF), which illustrates how many drops land at or within any given distance. In this case the disturbance function offsets the target point so that it gets closer to the mean landing point, giving smaller errors in general. The fact that the mean landing point with turbulence is close to this target point signifies that the addition of turbulence might not affect the average landing position substantially for head-wind releases, even though there is a large spread of individual landing positions.

The results from similar simulations with a tailwind release can be seen in Fig. 4.7. In this case, the disturbance function also appears effective in aligning the target point with the mean landing position. Based on the CDFs for both drop directions, the errors generally also decrease with the use of the disturbance function. In both scatterplots, the largest deviations from the mean occurs in the direction of the wind. One possible explanation for this phenomenon is that an increase in the wind speed affects the package more than a decrease as the drag force is proportional to the square of the relative velocity.

The metrics used to compare the results for different values are the mean errors, the errors within which 95 % of the simulations land, as well as the maximum errors. The values for the maximum errors gives an idea of what the worst case scenario could be, but it is unlikely that the actual worst case scenario appears in 1000 simulations, why the graphs for the maximum can be less smooth than for the aggregate graphs. In Fig. 4.8, the errors are shown when each variable is varied individually under

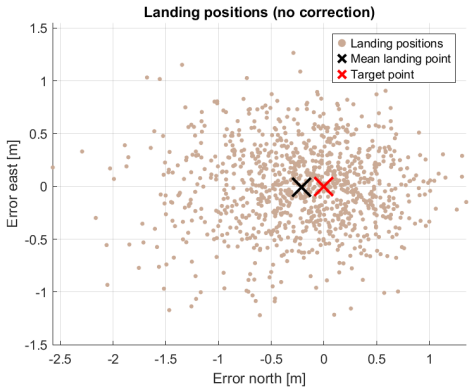

(a) Disturbance function not used. The mean landing point is at [-0.215 m, 0.008 m] compared to the target point.

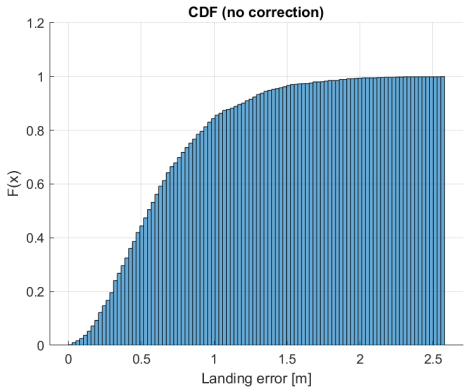

(b) Cumulative distribution function for simulation without disturbance function applied.

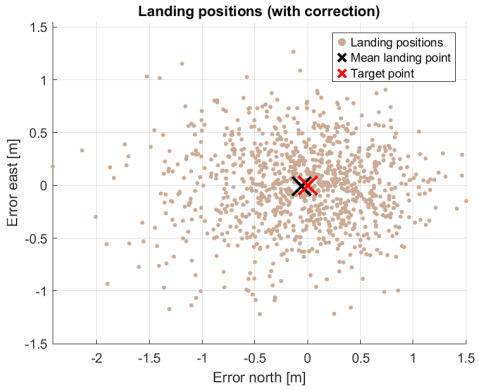

(c) Disturbance function used. The mean landing point is at [0.061 m, 0.002 m] compared to the target point.

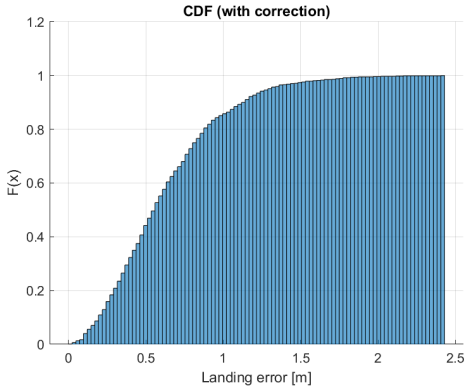

(d) Cumulative distribution function for simulation with disturbance function applied.

Figure 4.6: Simulations showing a scatter plot over the landing positions for 1000 isolated drops with turbulence for a headwind release with a wind speed of 15 m/s south, and an initial package velocity of 6 m/s north. All other variables are assigned their default values such that the disturbance function has values for this exact combination stored.

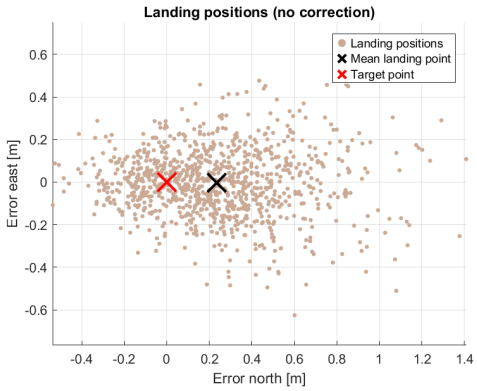

(a) Disturbance function not used. The mean landing point is at [0.235 m, -0.003 m] compared to the target point.

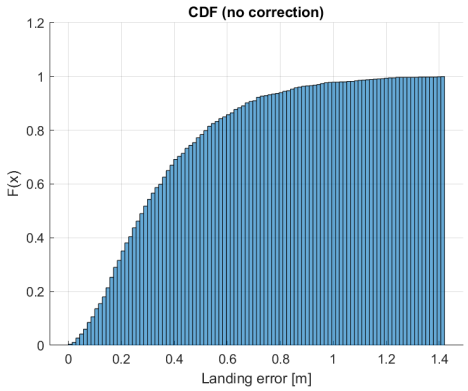

(b) Cumulative distribution function for simulation without disturbance function applied.

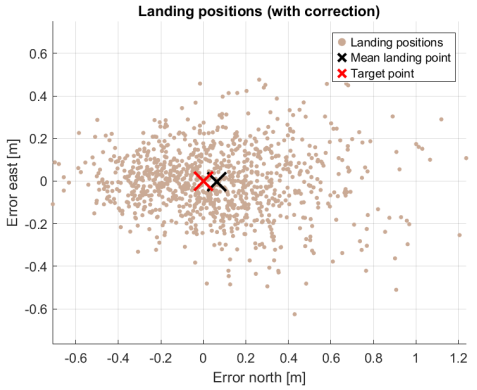

(c) Disturbance function used. The mean landing point is at [0.063 m, -0.003 m] compared to the target point.

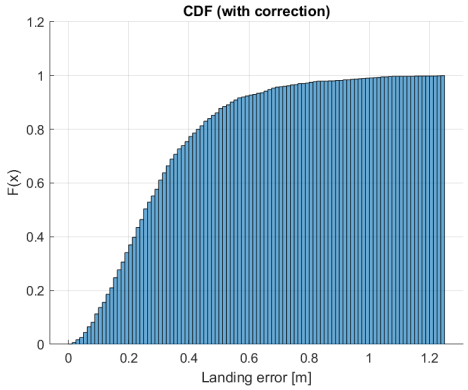

(d) Cumulative distribution function for simulation with disturbance function applied.

Figure 4.7: Simulations showing a scatter plot over the landing positions for 1000 isolated drops with turbulence for a tailwind release with a wind speed of 15 m/s north, and an initial package velocity of 6 m/s north. All other variables are the default values such that the disturbance function has values for this exact combination stored.

turbulent conditions, both with and without the disturbance function applied. The errors caused by the turbulence are large compared to the ones resulting from the imprecision of the analytical approximation.

4.1.3.1 Varying Variable not in Disturbance Function

When varying one of the variables that is not a variable in the disturbance function, it was previously seen that the correction was approximately 4 cm, if the other variables were kept at default. This gives a maximal difference possible between the graphs with and without disturbance function applied. This maximum occurs when the target point is moved fully in the direction of the landing point - or directly opposite it - for all simulations used to calculate the value. On average, whether the disturbance function increases or decreases the errors is expected to align with the results without turbulence (see Fig. 4.2). The 95th-percentile errors appear to align with this prediction, but the maximal errors are most often larger with the disturbance function applied.

The errors from the turbulence appear to be nearly linearly increasing with the drop height. This could be explained by the package being exposed to wind for a longer time. Comparing the results for a drop height of 3 m and 5 m, the 95th-percentile error almost doubles, with an absolute difference in order of decimeters. Therefore, as earlier assumed, it would be beneficial to release the package from as low a height as possible, with even small differences making an impact.

For the package's initial vertical velocity, it can be seen that larger positive values (downward) gives smaller errors. This could also be explained by the fact that if the package already is moving toward the ground, it takes a shorter time to land, giving the wind less time to act on it. However, utilizing this information to increase the accuracy of the delivery methods is difficult. For the fly-by, it might be possible to approach the target point with gradually decreasing altitude. This would however either result in the drone flying at a higher altitude to begin with, or risk colliding with the recipient. For the circular delivery, similar ideas would be likely to disrupt the package's controlled path.

For the vertical wind velocity, the errors are somewhat smaller for downdrafts. The difference though is small unless the wind is very large. The only way this could be controlled would be to not release the package for certain vertical wind velocities.

4.1.3.2 Varying Variable in Disturbance Function

For the package's horizontal velocity one can find the minimal error for a velocity between between -5 and -10 m/s. As the default value for the wind speed is 7 m/s in the direction opposite the package's velocity, it is likely that the minimum would correspond to this value. At this point, the relative velocity between package and wind would initially be purely vertical. With the drag force pointing in the direction opposite the relative velocity, this could result in small disturbances in the horizon-

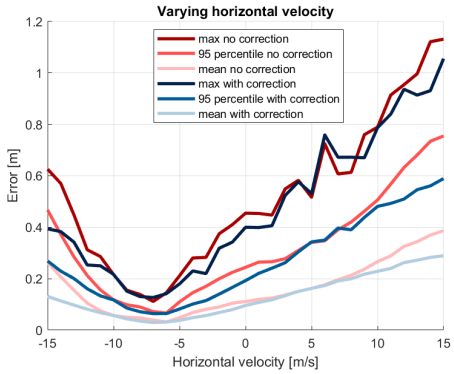

(a) Varying the package's horizontal velocity

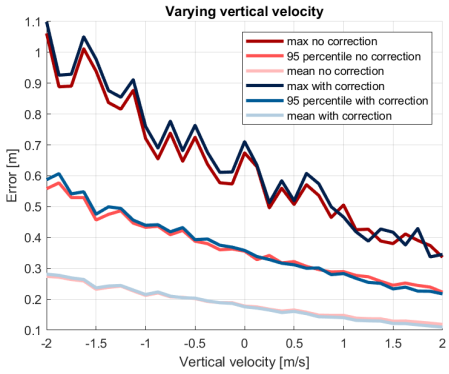

(b) Varying the package's vertical velocity

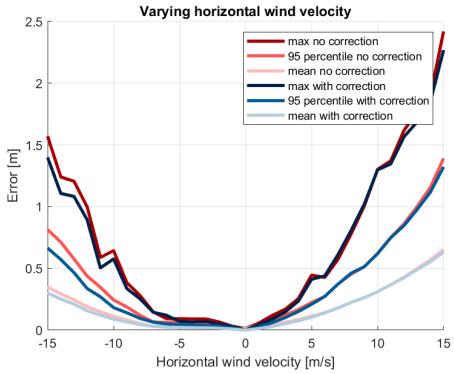

(c) Varying the wind's horizontal velocity

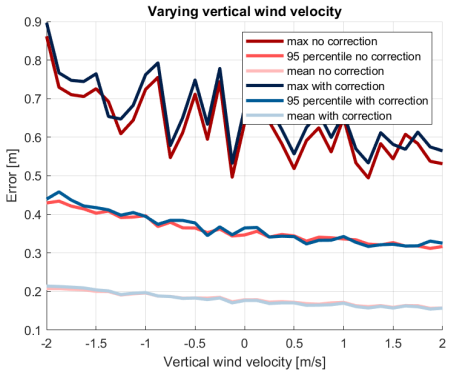

(d) Varying the wind's vertical velocity

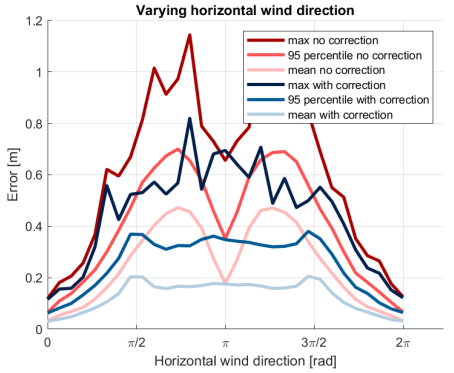

(e) Varying the angle between the velocities

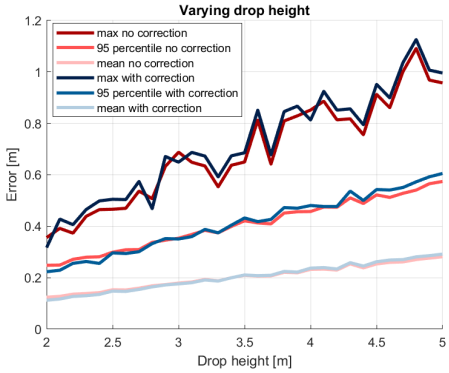

(f) Varying the package's initial height

Figure 4.8: Simulations comparing the errors, for isolated drops, with turbulence. For each value, 1000 simulations are done, and then the mean, 95 percentile and maximum errors are calculated both with and without a disturbance function applied. The parameters not varied are assigned to the defaults listed in Table 3.1. Note that due to the default angle of π rad, either a negative package or wind velocity represents a tailwind release. Also note that the positive vertical direction is downward.

tal plane.

For the horizontal wind speed, one can see a minimum at 0 m/s. This is explained by the turbulence intensity being zero in the absence of horizontal wind. More interestingly, another minimum is seen slightly below −5 m/s. This could correspond to the horizontal initial velocity of the package (i.e. 7 m/s in the opposite direction) and be explained with a parallel argument as for the minimum for the package velocity.

Not only can the minima be found at negative values in both graphs; the error is always smaller for the negative values than their positive counterparts. This suggest that one can obtain a better precision when releasing the package tailwind than headwind. However, this requires the ability to release the package with the same initial velocity in both cases, which may be more feasible with the circular delivery method than with a fly-by. In both graphs it can also be seen that the disturbance function helps decrease the errors, even though turbulence is the largest source of error.

In the simulations varying the angle, it can again be seen that the errors are smaller when releasing tailwind than headwind, with large differences in the order of decimeters. The disturbance function also improves the accuracy for all values. This is especially important when releasing the package headwind, as it can remove the volatility that could otherwise be seen close to π rad.

4.1.4 Landing Velocity with Turbulence

In addition to the accuracy, one other factor that is important in determining whether to release the package headwind or tailwind is the package velocity at landing. If the velocity is too high, either the package or the recipient could get hurt on impact. In Fig. 4.9 one can see the mean, 95th-percentile and maximum velocities when varying one variable at a time. Compared to other variables, the impact of vertical velocities on the impact velocity is small. Unsurprisingly, the impact velocity increases with increasing drop height. The simulations varying the drop height are performed with a headwind release, so the velocity with a tailwind difference is expected to be even larger. This gives one more reason to drop the package from as low a height as safe and possible.

The most important decision to limit the velocity is whether the package is released headwind or tailwind, which can be seen in the graphs for the horizontal velocities as well as the one for the angle between them. It is easier to control the initial velocity of the package than the average wind speed. Assuming that it is possible to keep the initial horizontal speed of the package close to 6 m/s - which is the expected velocity in the circular delivery - the most relevant results is when the horizontal wind speed is varied. For wind velocities with an absolute value below 10 m/s the relation between the impact velocity and the wind velocity appears linear with lower landing velocities for headwind drops. For headwind drops, there is a

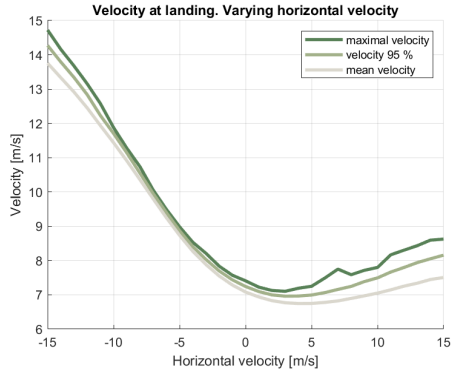

(a) Varying the package's horizontal velocity

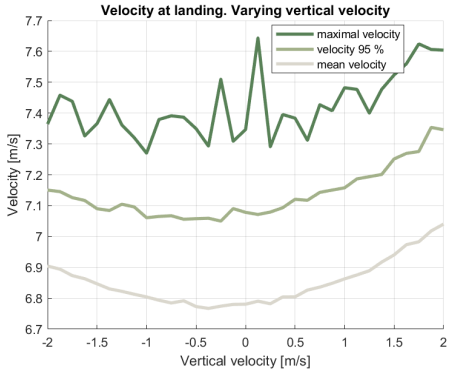

(b) Varying the package's vertical velocity

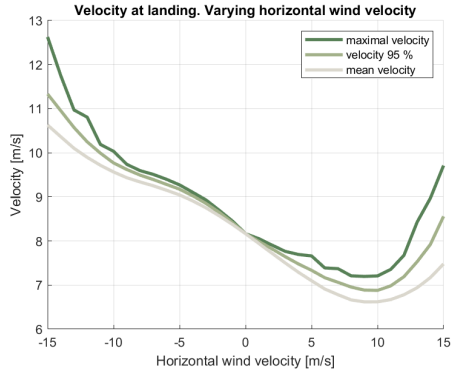

(c) Varying the wind's horizontal velocity

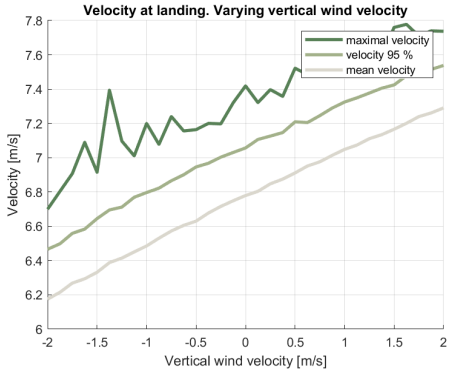

(d) Varying the wind's vertical velocity

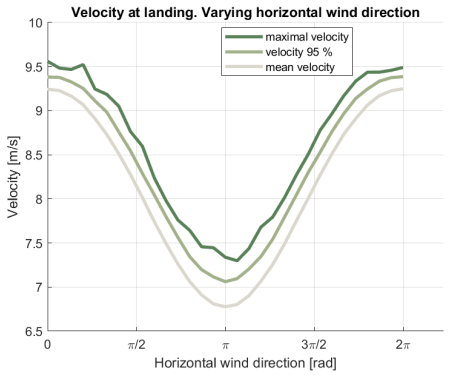

(e) Varying the angle between the velocities

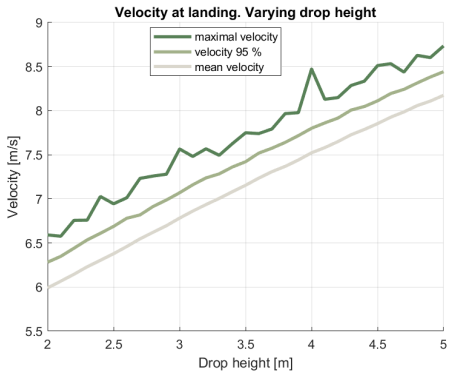

(f) Varying the package's initial height

Figure 4.9: Simulations comparing the landing velocities, for isolated drops, with turbulence. For each value, 1000 simulations are done, and then the mean, 95 percentile and maximum velocities are calculated. The parameters not varied are assigned to the defaults from Table 3.1. Note that due to the default angle of π rad, either a negative package or wind velocity represents a tailwind release. Also note that the positive vertical direction is downward.

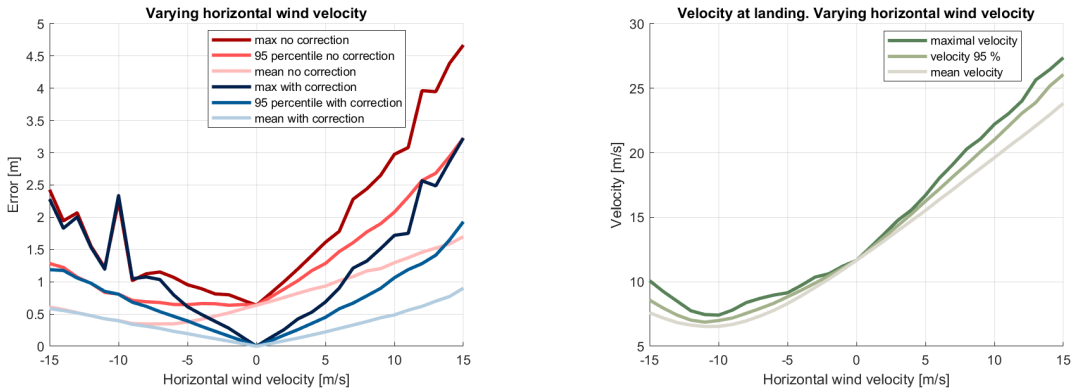

(a) Errors **(b)** Landing velocity

Figure 4.10: Simulations showing the errors and landing velocities for different wind velocities for isolated drops where the package is released with an airspeed of 20 m/s. For each value 1000 drops are done.

minimum close to 10 m/s after which the velocity quickly increases. The minimum probably corresponds to where the wind speed is precisely enough to stop the horizontal movement right before the fall. For higher horizontal wind speeds (or greater drop heights), the package begins to gain horizontal speed in the direction opposite to its initial velocity. At even higher wind speeds, the landing velocities are likely to be more similar for both headwind and tailwind releases.

Determining whether to drop the package headwind or tailwind is a matter of prioritizing either the accuracy or the landing velocity. This decision could be based on parameters such as the mass and fragility of the package as well as whether or not the recipient can take cover to avoid being hit on impact.

4.1.5 Isolated Falls with Constant Initial Airspeed

Some of the conclusions from the previous sections are more applicable to the circular delivery than the fly-by delivery. This is a consequence of the horizontal package velocity being more dependent on the wind speed in this method. Therefore, simulations with isolated falls are also done where the package is always released with a horizontal airspeed of 20 m/s, to emulate the conditions for the fly-by delivery. The results from these simulations can be seen in Fig. 4.10. These simulations are done with a new disturbance function, generated with all integer values for the horizontal wind velocities in the range [-15, 15], and all horizontal package velocities in the range [0, 35]. For the angle only one value was used, but as the wind takes both positive and negative values, this covers both the angle of 0 rad and π rad.

The accuracy is better when releasing the package headwind than tailwind, as seen in Fig. 4.10. This is contrary to previous conclusions, and is likely because of the fact that the package is dropped with a lower ground speed for this case, resulting in smaller disturbances. Releasing the package headwind, it is possible to predict where the package lands within one meter for most wind speeds. However, when

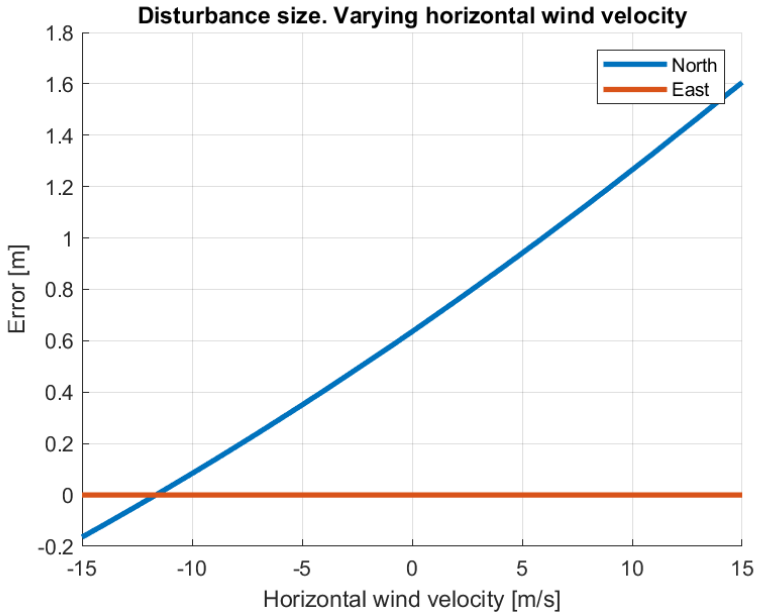

Figure 4.11: The plot shows the size of the correction from the disturbance function when the package is released with an airspeed of 20 m/s for different wind speeds. Both the initial package velocities and the wind velocities are fully along the north axis.

adding the other parts of the fly-by algorithm, further sources of error are added.

The size of the correction from the disturbance function can be seen in Fig. 4.11. The correction follows a linear relation where the maximal correction for the given parameters is roughly 1.6 m. As these simulations attempts to emulate the conditions for the fly-by delivery, one would expect similar outputs from the disturbance function using that algorithm.

4.2 Fly-by Delivery Method

For the fly-by algorithm, it is important to choose a suitable threshold error for the release mechanism (see Section 3.4). With a too low threshold, the algorithm often does not find a suitable opportunity to release the package, but with a too high threshold the package might be released even if it is expected too far from the target. If the algorithm never finds a suitable time step to release the package, the drone can return and try again. A package that lands in the water, however, may be irreparably damaged or difficult to retrieve. The simulation handles situations when the algorithm fails to drop the package by running the simulation anew, and counting how many attempts have failed. A threshold of 1 m was chosen as a compromise between accuracy and drop-rates. More thorough research are necessary to determine a suitable threshold more precisely.

Simulations are done both with the same disturbance function as in Section 4.1.5,

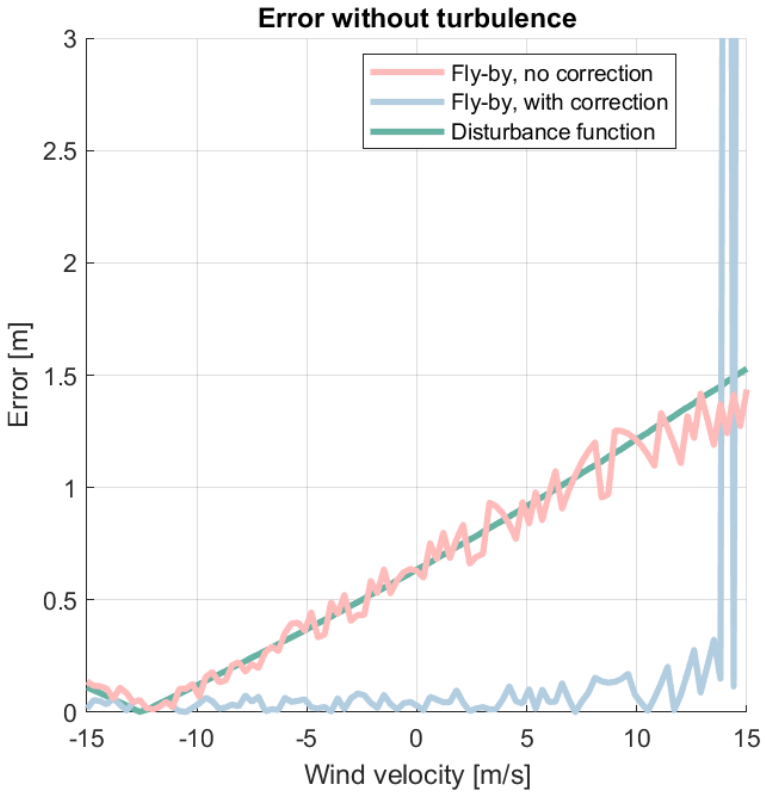

Figure 4.12: The errors from the fly-by drops without turbulence. For all wind values the drone's control system tries to keep an airspeed of 20 m/s and a height of 3 m. The simulation is repeated both with and without the use of the disturbance function. Alongside these, the predicted disturbance from the disturbance function, with exact values and no drone, are also shown. Using the disturbance function gives a smaller error for most values, but it has some spikes for wind speeds slightly below 15 m/s. These spikes are shooting outside the limits of the graph to a maximum error of 10.1 m.

and with no disturbance function at all. As an initial verification of how well the release mechanism works, simulations without turbulence are done with the drone targeting an airspeed of 20 m/s (see Fig. 4.12). The disturbance from the fly-by without correction correlates closely with the predicted error from the disturbance function. When the disturbance function is included in the simulations, the errors get substantially smaller for most values. Both with and without the use of the disturbance function, the values fluctuate around 0 and the output from the disturbance function, respectively. These fluctuations are expected as the optimal time step to release the package might not necessarily mean that the mechanism expects the package to land precisely at the target point; the optimal release time might be between two time steps or the drone's control system might be unable to keep the height and path exactly. With a smaller time step one could expect the size of the fluctuations to decrease.

One unexpected result is the spikes that can be seen for wind speeds slightly below

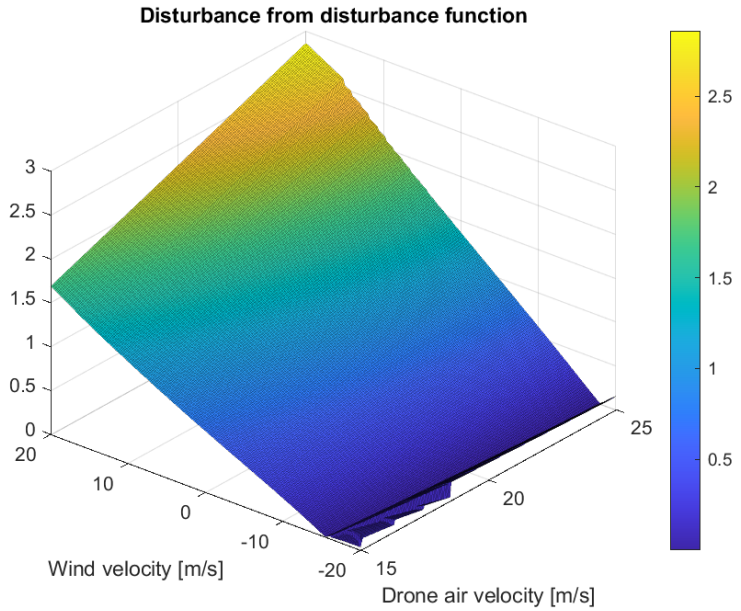

Figure 4.13: The norm of the disturbance from the disturbance function for different combinations of wind speeds and drone airspeeds close to the ones used for the fly-by simulations. For both variables 201 uniformly distributed values have been used. The maximum disturbance is roughly 2.86.

15 m/s. These spikes look unnatural and reach a maximum height of 10.1 m. This cannot be explained solely by the causes of error discussed in the previous paragraph. These should not cause errors larger than the threshold error of 1 m. One other idea would be if the disturbance function gives large outputs for some specific inputs. The fact that it only occurs when using the disturbance function gives credit to this being the case. To test this theory, the outputs from the disturbance function are studied for different inputs, the result of which can be seen in Fig. 4.13. Even if the velocities of the drone and the wind deviate with several meters from the simulation means, the disturbance function would not give an output with a norm larger than 3 m. Even if this maximum occurred and it was applied in the wrong direction, it would not be enough to explain the anomaly.

Another idea for the cause of the spikes is that it is a cause of numerical errors in the simulations. This would imply that they can happen even without the disturbance function applied, and that it is a coincidence that it has so far only appeared with it applied. Regardless of explanation, the values for large positive wind speeds should be observed more skeptically for the fly-by results.

The next step is to perform the simulations with turbulence. The results for this can be seen in Fig. 4.14. For large negative wind speeds the disturbance function is only expected to give an offset of approximately 1 dm, which would barely be visible in the graph. As the disturbance function is the only methodical difference between the simulations, the difference between the graphs can largely be attributed to the stochastic behavior of the wind. For positive wind velocities, it can be seen that the

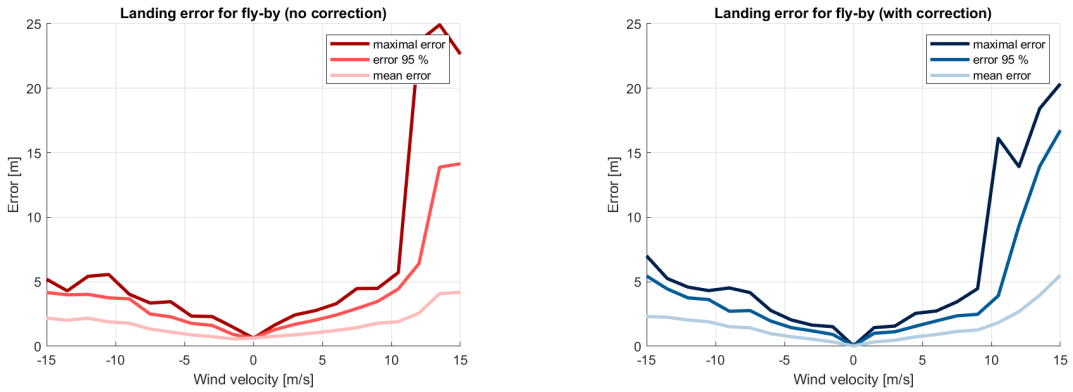

(a) Results from fly-by drops without disturbance function.

(b) Results from fly-by drops with disturbance function.

Figure 4.14: Errors when delivering a package using a fly-by drop. The drone's controller tries to keep a constant airspeed of 20 m/s and the drone is approaching the drop point in a direction parallel to the wind. This means that negative wind speeds signify a headwind release and positive winds a tailwind drop. For each value 100 drops are made, both with and without a disturbance function.

95th-percentile errors are smaller with the disturbance function applied than without. This result align with the fact that the output from the disturbance function grows with increasing wind velocity. This difference could partially also be caused by the stochastic behavior of the wind. To observe this more clearly, one can study a scatterplot of the landing positions in both cases (see Fig. 4.15). With the use of the disturbance function, the mean landing position gets significantly closer to the target, proving that the disturbance function has the intended effect.

One would expect this difference to increase for even higher tailwinds as the size of the disturbance function then increases. Instead, the errors increase drastically, both with and without the disturbance function, from about 10 m/s. This sudden increase could align with the previous findings of large spikes for high tailwinds with the use of a disturbance function. As the same phenomenon is observed for both cases, the previously found spikes can be assumed not to be caused by the disturbance function itself. If the spikes are indeed caused by a numerical error or some other bug, one could, based on previous patterns, expect that the errors would in reality continue on a near-linear trajectory even for these values, and that the difference with and without the use of the disturbance function would increase.

Comparing the errors for headwind and tailwind drops, the errors are similar with the use of the disturbance function, apart from the area with the sudden increase in errors. The errors from the fly-by can likely be reduced by selecting the drone's target airspeed more carefully and adjusting it based on wind velocity — allowing for lower airspeeds in lighter winds, which may result in improved drop accuracy.

In general, the errors are significantly larger for the full algorithm than for the iso-

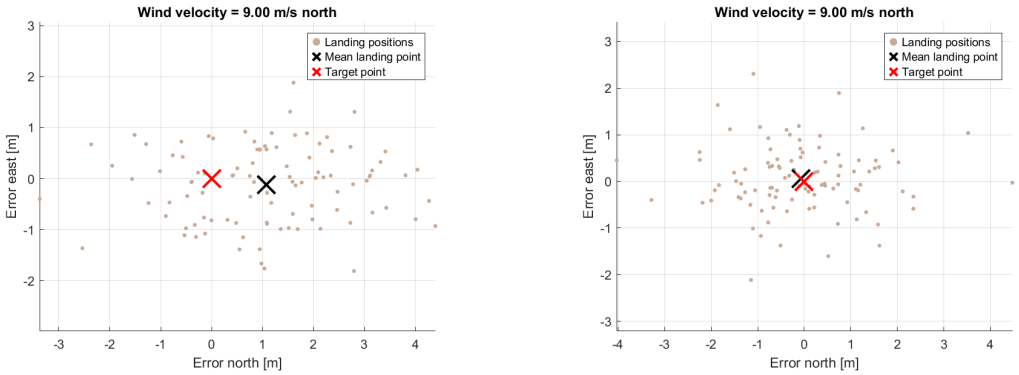

(a) Scatterplot without disturbance function. Mean landing position is at [1.08, -0.12] compared to target point.

(b) Scatterplot with disturbance function. Mean landing position is at [-0.07, 0.06] compared to target point.

Figure 4.15: Scatterplot of landing positions for the fly-by algorithm with and without disturbance function. In both cases the drop is perform in a 9 m/s tailwind.

lated drops for the same values (compare Fig. 4.10a and Fig. 4.14b). The release mechanism could contribute an error up to about the threshold error of 1 m. The difference however is about 1 m for the mean and 4 m for the 95th-percentile errors, so that is not the only reason for the increase. Another source of error is the drone's inability to perfectly control its path, which may cause deviations in the package's height and velocity direction at the time of release.

Based on these results, the errors in the 95th-percentile are above the target accuracy of 1 m even for lower wind velocities. To study with what accuracy the algorithm can deliver packages within certain distances the CDFs can be observed for different wind speeds (see Fig. 4.16). For small wind speeds of 4.5 m it is possible to land within 1 m of the target almost 80 % of the time, regardless of drop direction. This accuracy is insufficient for trusting in the algorithm. For larger wind velocities, the accuracy is decreased further and the package seldom lands within the 1 m range. For tailwind releases in 15 m/s wind, the results initially follow a curve similar in shape to those for lower wind speeds. However, a large portion of the data is later spread over a significantly wider range, providing further evidence that the large errors stem from an issue occurring in some of the simulations.

Another important measure is the velocity of the package when it lands. The results for this can be seen in Fig. 4.17. It can be seen that the landing velocities differ substantially based on the wind velocity. For headwind drops the mean landing velocity is smaller than for the tailwind drops in the same wind speed. This could in large part be due to the ground speed of the package being larger upon release for tailwind releases. The effect of this could be mitigated if the drone was always targeting the same ground speed for each wind speed.

For headwind drops, the velocities initially decrease, but after -5 m/s they stay close to constant, with a slight increase towards the end. The relative velocity, as

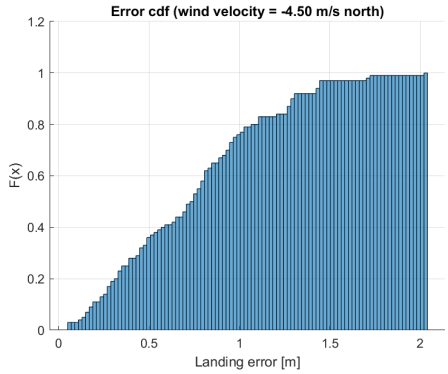

(a) Headwind release with a wind speed of 4.5 m/s southward.

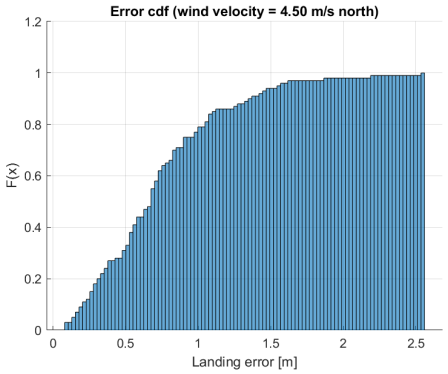

(b) Tailwind release with a wind speed of 4.5 m/s northward.

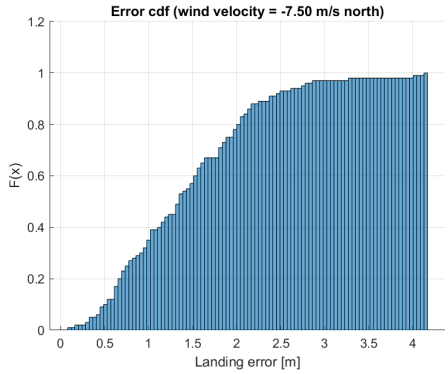

(c) Headwind release with a wind speed of 7.5 m/s southward.

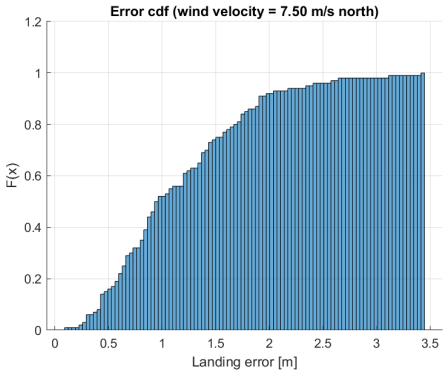

(d) Tailwind release with a wind speed of 7.5 m/s northward.

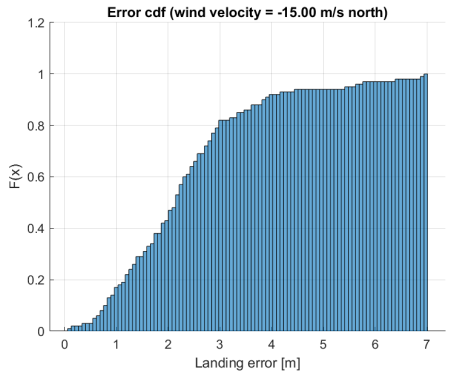

(e) Headwind release with a wind speed of 15 m/s southward.

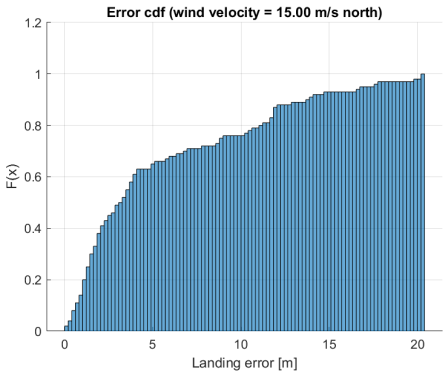

(f) Tailwind release with a wind speed of 15 m/s northward.

Figure 4.16: CDFs for the fly-by drops with the disturbance function applied for some different wind speeds. In all cases the drone maintains an airspeed of 20 m/s northward. The x-scales extend to the maximal errors observed for each case.

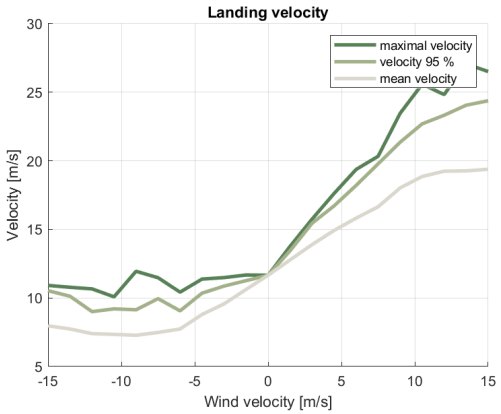

Figure 4.17: The mean, 95th-percentile and maximum velocities for 1000 simulations per value when delivering packages with a fly-by drop.

well as the drag forces, are equal at the time of release for all velocities. One would expect that there is a minimum where the wind just about manages to stop the horizontal movement (compared to the ground) of the package, after which its velocity is expected to increase. This could occur close to a wind velocity of $-10\,\mathrm{m/s}$, explaining the small differences observed.

A third parameter that could be of importance in evaluating the fly-by delivery, is the time taken to deliver the package, and how often the algorithm manages to drop the package to begin with. The results for this can be seen in Fig. 4.18. The time is clearly larger for the larger headwinds. This should be caused by the drone's higher ground speed for larger wind speeds, allowing it to faster clear the distance to the drop point. The time necessary to fly a certain distance is expected to be proportional to the inverse of the ground velocity, and the graphs do have a similarity to the graph of $1/x$.

The success rate is also an important factor. Turning around to make another approach is more time-consuming than the time difference between the different drop directions. The success rate is higher for headwind drops, possibly because the ground speed is lower in this case. As a result, the drone covers less distance between time steps, increasing the number of steps during which it is within the threshold error range. This, in turn, makes it more likely to find a suitable release time. Based on this conclusion, the success rates could be increased by using a shorter time step. Another way would be raising the threshold error, but this would come at expense of the accuracy.

Based on the fly-by simulations the accuracy is similar whether the package is released headwind or tailwind, except for wind speeds of approximately $10\,\mathrm{m/s}$ or above, where unexpectedly large errors are recorded for the tailwind drops. The package's velocity at landing can, at average wind conditions, be halved by releasing the package head-wind. In addition, it is more likely that the algorithm will succeed with the drop for the headwind drop. So using this methodology, it is over-

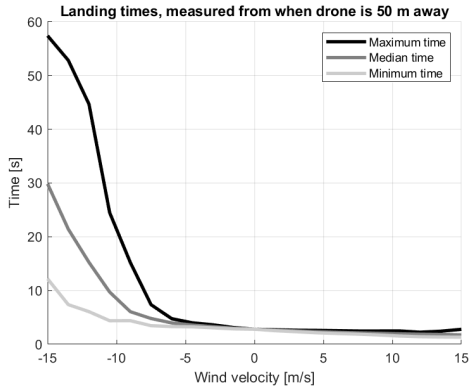

(a) The time it takes for the algorithm to perform a drop, measured from when the drone is 50 m away from the target. Simulations when the algorithm does not drop the package is excluded.

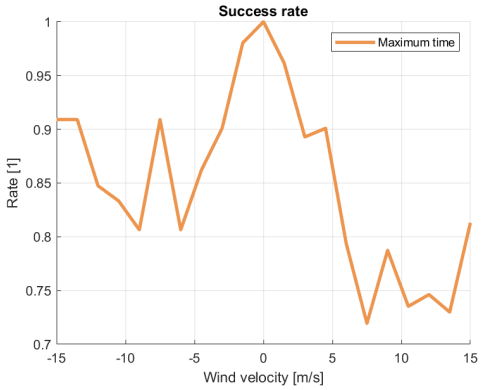

(b) The rate at which the release mechanism finds a suitable time step to drop the package, regardless of how close it lands. For each value the simulation runs until 100 successful drops have been performed.

Figure 4.18: Measures for how quickly the algorithm is able to perform the drop. If the drop fails, the drone would have to turn around and approach the target point once again, increasing the time.

all beneficial to drop the package headwind. For average wind speeds, the algorithm manages to land within a meter of the target point 40 % of the time. To accurately drop the package with a 95 % certainty, the requirement would need to be raised to ≈ 3 m.

4.3 Circular Delivery Method

In order to determine if the circular delivery method is viable, several variables used must be calibrated. This is achieved by smaller simulation batches where three different values of one variable are paired up with three different values of another variable, then each of the nine pairings are simulated 100 times in order to get an understanding of which values should be used. The tested variables are: drone airspeed, rope length, number of passes and threshold error. Number of passes indicates how many times the drone should circle the target before executing the offset function as described in Section 3.6.5. Each attempted drop is timed from when the drone is 100 meters from the target until the package lands, for the big batch simulations of 1000 the distance is 50 m. If the simulation runs for 400 s without finding an opportunity to drop the package, it is considered a failed drop. When the package is dropped, if it lands within the target area, defined as a circle with a radius of one meter, it is considered a successful delivery. The default values used for the simulations can be seen in Table 4.1.

For each simulation batch, two plots are made. The first plot shows the landing

Table 4.1: Standard values used for the circular delivery simulations.

Variable	Value
Drone airspeed	18 m/s
Rope length	60 m
Average wind speed	8 m/s
Number of passes	6
Threshold error	0.6 m
Time step	0.001 s

position of each successful drop for each pair of tested variables. To aid in the interpretation of the plot, a circle with a radius of one meter is shown to represent the target area surrounding the target, each dot inside the circle represents a successful delivery. The mean time per drop is also displayed. These plots are all presented in the Appendix Section A.1. The second plot consists of a CDF showing the errors for each successful drop. To aid interpretation, the percentage of successful drops, the mean error, as well as the mean delivery time for the successful drops are shown.

The goal of the first simulation is to determine which rope length in combination with which drone speed gave the best result in terms of reliability and accuracy. The tested drone speeds are 18, 22 and 26 m/s, the chosen rope lengths are 30, 45 and 60 m. The resulting cumulative CDF of the resulting error or each successful drop can be seen in Fig. 4.19. In this figure we see that only two combination of values, those being 18 m/s with 60 m and 22 m/s with 45 m, led to all of the successful drops landing within 1 m of the target resulting in successful deliveries. However, out of these to combinations, the later also resulted in a 100 % successful drop rate as well as a lower mean error. And while the average time was 30 s higher, we determine that the optimal drone speed and rope length to be 22 m/s and 45 m.

The second simulation batch was done to compare the number of circulations for the offset function with the threshold error. For this purpose, the threshold error values of 0.3, 0.6 and 0.9 m are tested, while the number of circulations tested are 1, 3, and 5. In Fig. 4.20 the resulting CDF is once again shown. From the CDFs we see three combinations of values where all successful drops were successful deliveries. The combinations were thresholds of 0.3, 0.3 and 0.6 m in combination with offset circulations 3, 5, and 5 respectively. Out of these combinations the highest successful drop rate is achieved by the threshold error of 0.6 m and 5 circulations at 99 %. While this combination results in the highest success rate, it does result in the highest mean error of the three. We believe that reliability is more important than accuracy as long as the package lands within 1 m of the target. Furthermore, this combination of values also result in the lowest mean time. These values are therefore chosen for later simulations.

Based on the previous simulations, the following are chosen for further simulations: 22 m/s drone airspeed, 45 m rope length, 0.6 m threshold error and 5 circulations for the offset function. The wind speed was updated to 10 m/s in order to apply

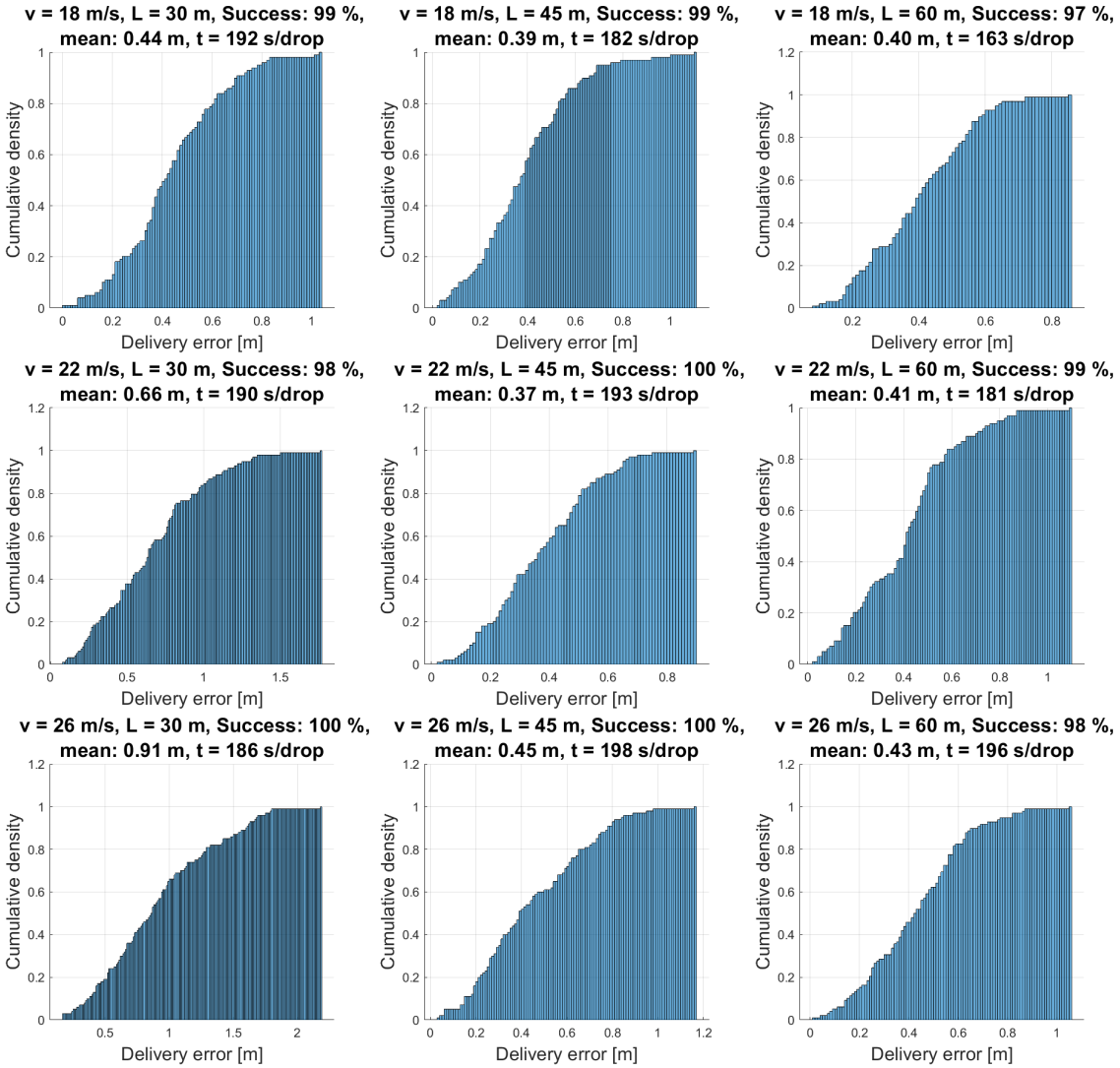

Figure 4.19: CDF for all successful drops for different values of airspeed (v = 18, 22 and 26 m/s) and rope length (L = 30, 45 and 60 m). The success rate denotes how many attempted drops were successful. For each pair of values 100 simulations were run.

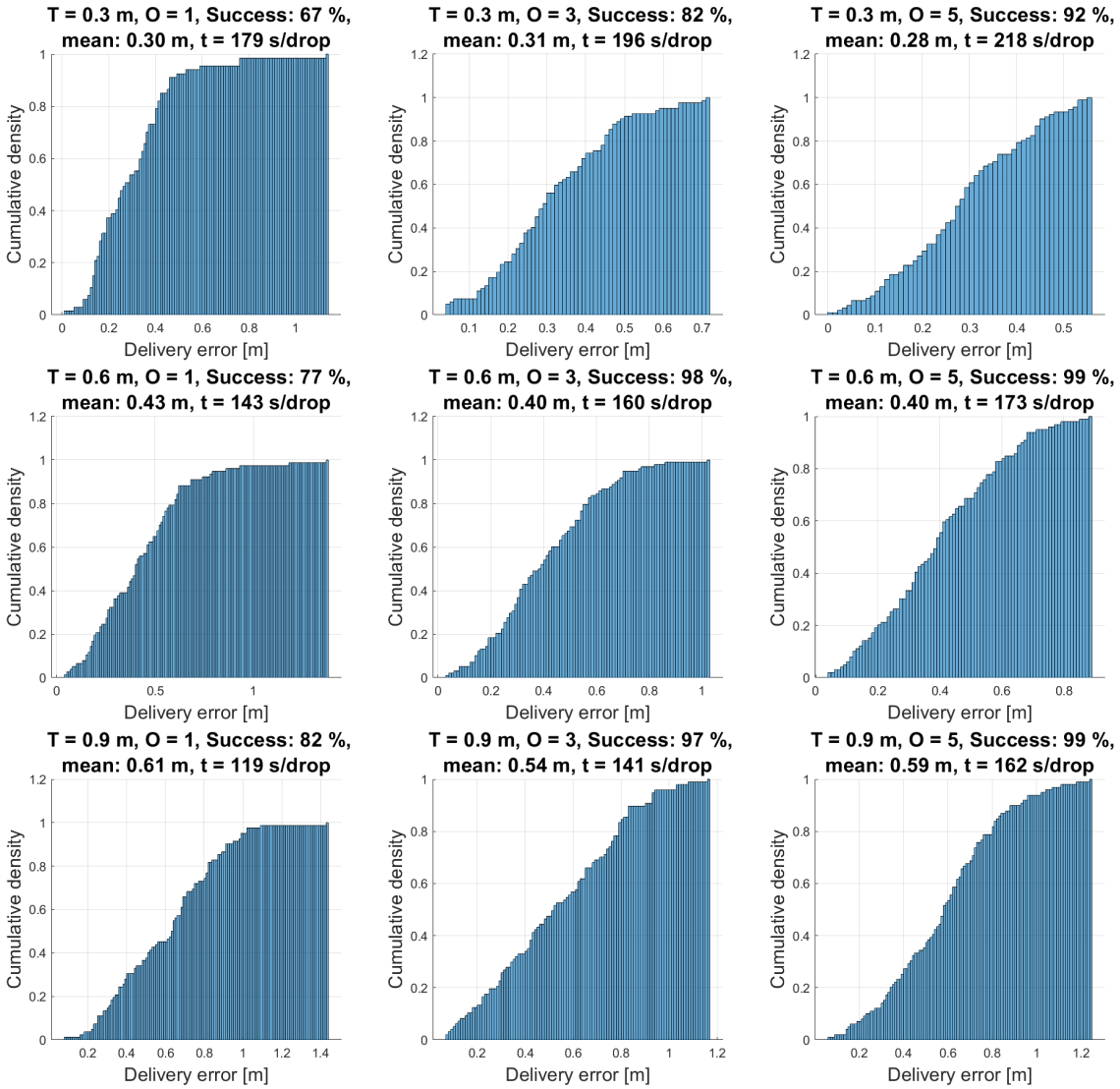

Figure 4.20: CDF for all successful drops for different values of threshold error (T = 0.3, 0.6 and 0.9 m) and offset circulations (O = 1, 3 and 5). The success rate denotes how many attempted drops were successful. For each pair of values 100 simulations were run.

more stress to the simulation than the average wind situation would. A simulation with these values is done. During the simulation a total of 1000 attempted deliveries are made in order to collect more reliable data to investigate the feasibility of this delivery method.

First, 1000 attempted deliveries are simulated without the use of the disturbance function. The resulting cumulative CDF can be seen in Fig. 4.21. In this figure we see that 98.2 % of attempted drops were successful, and of those 97.3 % resulted in a successful delivery as they landed within 1 m of the target. This means that each attempted delivery has a total chance of 95.5 % to be a successful delivery. The package's velocity at landing was at maximum 8.4 m/s, 95th-percentile 8.0 m/s and on average 7.7 m/s.

In an attempt to increase the accuracy, the disturbance function was implemented and another 1000 attempted deliveries are made. The results are presented in Fig. 4.24. This time we see that 98.6 % of attempted drops succeed, and of those 95.7 % are successful deliveries. That gives a total success rate of 94.4 %. This represents an increase of 1.1 percentagepoints compared to the simulations without the disturbance function. Why we get worse results with the disturbance function will be explored in Section 4.4. One interesting comparison between the results is the maximum and mean error. Without the disturbance function, we get a maximum error of around 1.45 m and a mean error of 0.48 m. With the disturbance function, we get a maximum error of around 1.78 m and a mean error of 0.46 m. So with the disturbance function we get a higher maximum but a lower mean, which suggests that the deliveries that land within the 1 m area land closer to the target with the disturbance matrix compared to without it. The package's velocity at landing was at maximum 8.4 m/s, the 95th-percentile was 8.1 m/s and on average it reached 7.7 m/s. As expected, the disturbance function did not have a significant effect on the final velocity of the package.

The next simulation batch for the circular delivery method is a stress test, where the two variables varied are drone airspeed and wind speed. The velocities tested are: 18, 22 and 26 m/s and the wind speeds are 5 m/s to represent a gentle breeze, 10 m/s to represent a fresh breeze with slightly higher wind than average and lastly, 15 m/s to represent near gale conditions when the Swedish Meteorological and Hydrological Institute (SMHI) issues a yellow warning [13], [14]. The simulation also used the previously tested disturbance matrix. In Fig. 4.23 we see how the method performs under different wind conditions. In the first column we see that the method performs well in 5 m/s wind with all successful drops lands within 1 m of the target. In the second column we again see that the method performs well in 10 m/s wind with most deliveries resulting in a sub 1 m error. In the last column we see that the method starts to falter in the higher wind speeds of 15 m/s. The successful drops resulted in successful deliveries in 61 %, 68 % and 69 % for 18 m/s, 22 m/s and 26 m/s drone airspeed respectively. This shows that while the method works well in lower wind speeds it regularly fails in higher winds.

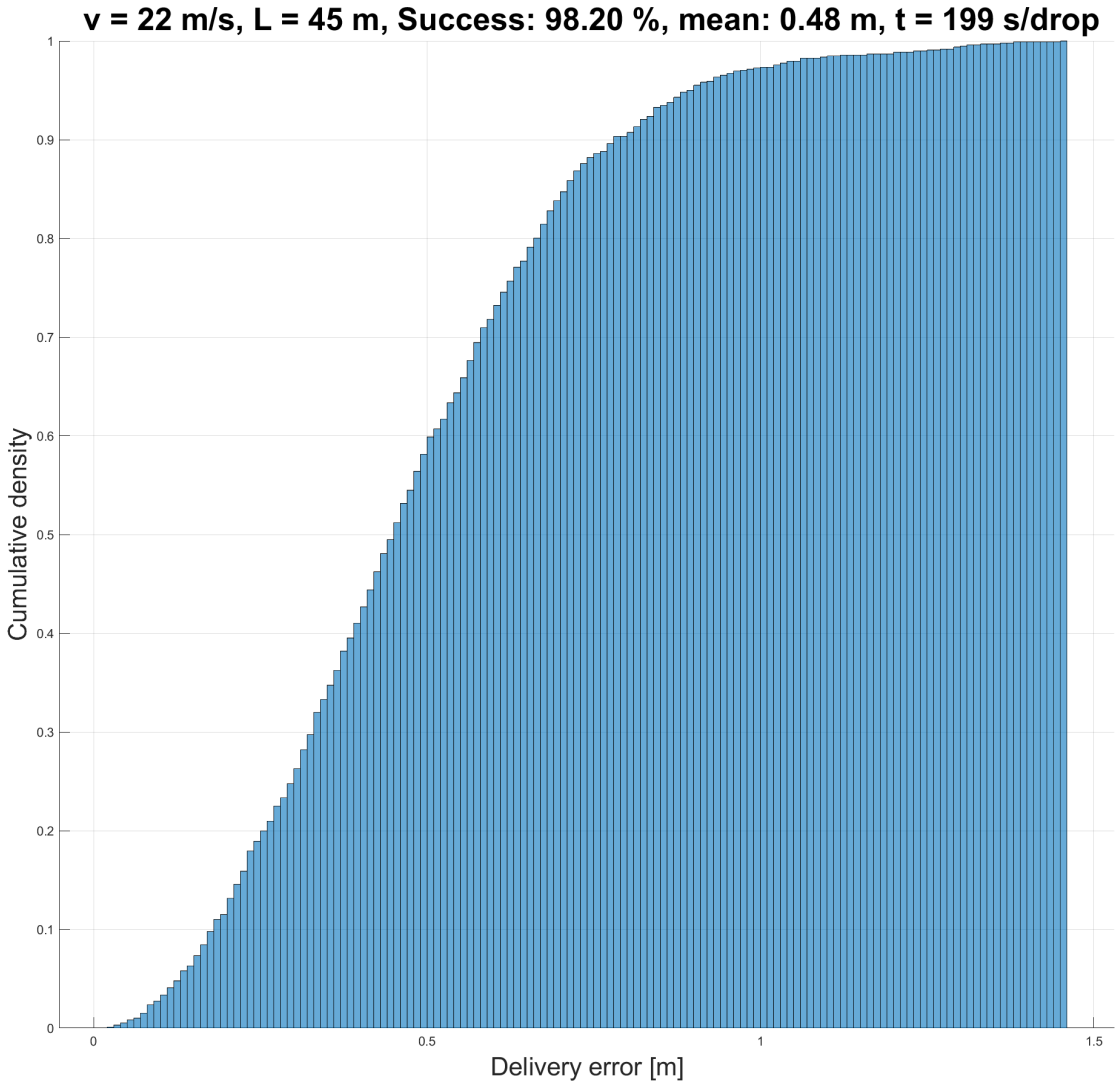

Figure 4.21: CDF for all successful drops for a larger simulation batch. A total of 1000 simulations were run with the values: drone velocity 18 m/s, rope length 45 m, average wind speed 10 m/s, number of passes 5 and threshold error 0.6 m. The success rate denotes how many attempted drops were successful.

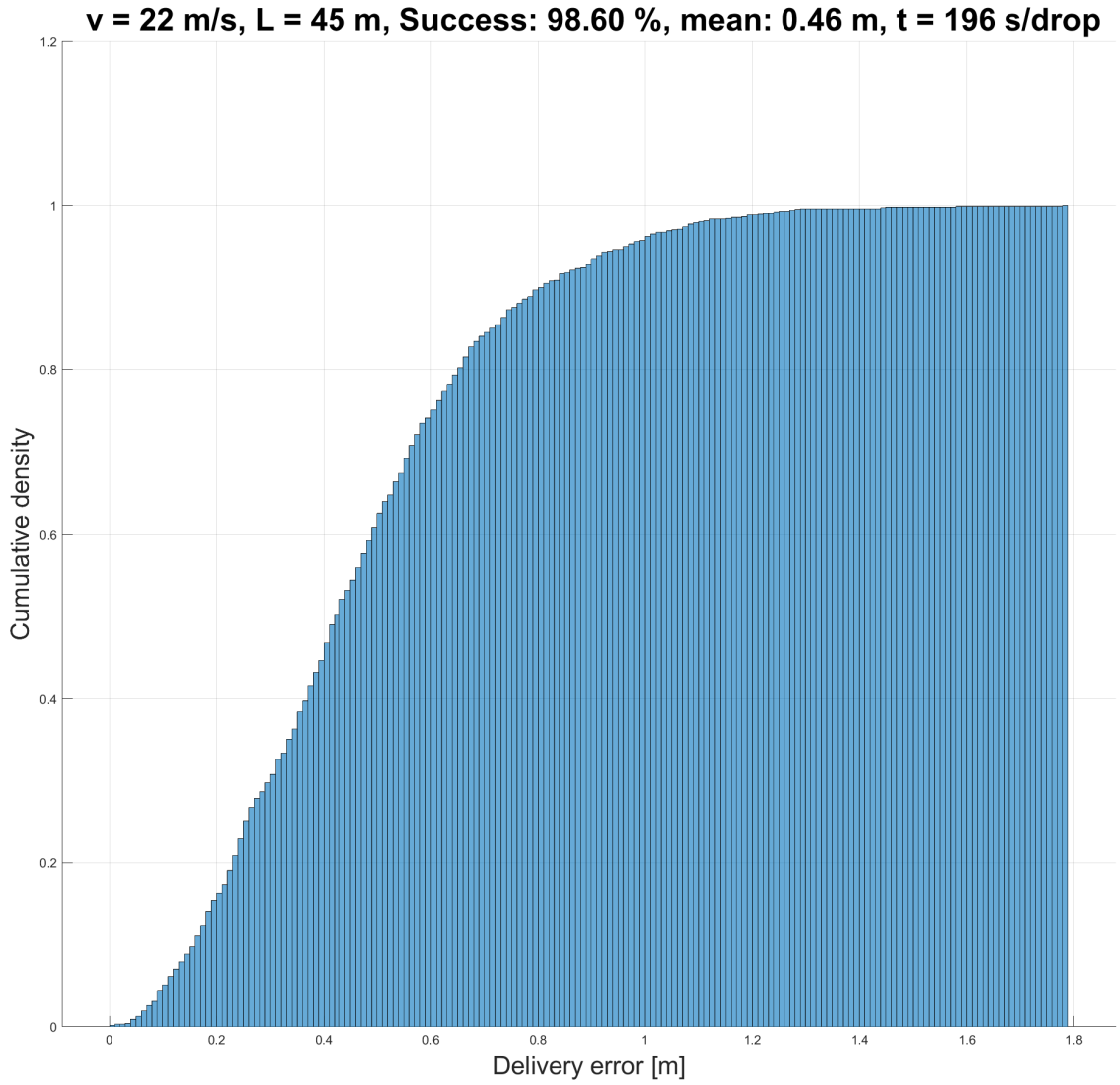

Figure 4.22: CDF for all successful drops for a larger simulation batch using the disturbance function. A total of 1000 simulations were run with the values: drone velocity 18 m/s, rope length 45 m, average wind speed 10 m/s, number of passes 5 and threshold error 0.6 m. The success rate denotes how many attempted drops were successful.

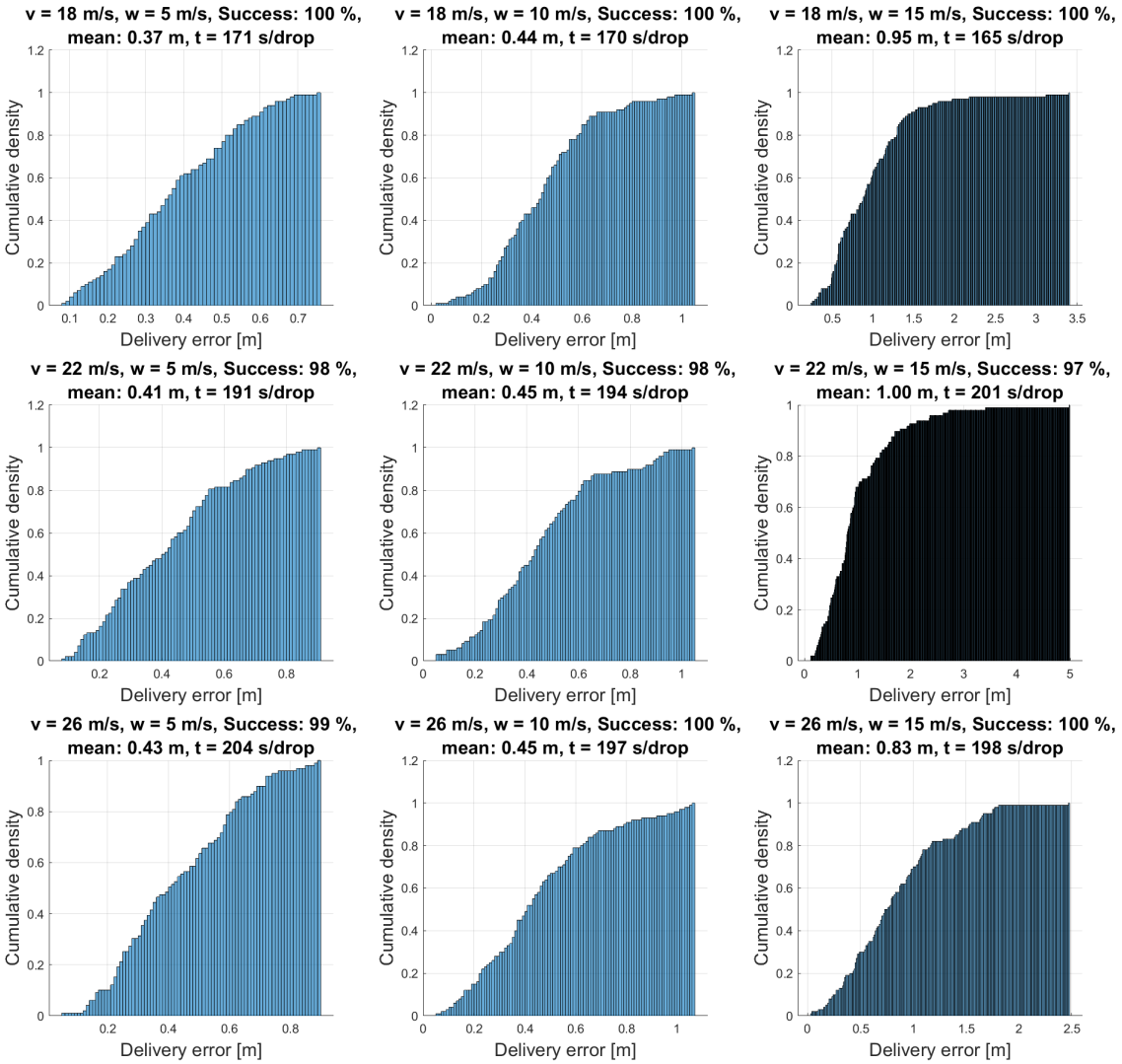

Figure 4.23: CDF for all successful drops for different values of airspeed (v = 18, 22 and 26 m/s) and wind speed (w = 5, 10 and 15 m/s). The success rate denotes how many attempted drops were successful. For each pair of values 100 simulations were run.

In the previously presented Fig. 4.8 we see that, for isolated falls, releasing tailwind instead of headwind should improve the accuracy for circular drops. So, for the last simulation batch, another 1000 simulations are run, this time attempting to release the package with the wind, contrary to the previous simulation batches. In Fig. 4.24 we see that 89.7 % of successful drops are successful deliveries. This is interesting as it contradicts the previous results. One possible reason as to why this is the case, is the angle at which the package is dropped. If we compare the average angle at which the package is dropped we get -0.0014 rad for the tailwind simulations and 0.0050 rad for headwind. These are good values as we want to release the package as close to 0 angle as possible. However if we compare the standard deviation we see a different picture. For the headwind we get 0.1372 rad while for the tailwind we get 0.1698 rad. Meaning that while the average are similar, for the tailwind the values deviate more from the average, resulting in larger angles at drop. If this larger standard deviation is caused by the package being released with the wind, it could partially explain the worse results.

4.4 Comparing Result Values

In Section 4.1.1 the resulting error was studied as it changed within a range. The ranges for each variable were: drop height, 2-5 m; horizontal velocity, –15 to 15 m/s; vertical velocity, –2 to 2 m/s; and angle, 0 to 2π radians. Wind is disregarded as it is outside of control. Now, with the final simulation of 1000 attempted deliveries completed, we can compare these ranges with the ranges collected from the simulation. Due to early tests showing a large effect on error from the vertical velocity of the package at drop, a manual range was implemented that stops the package from being dropped if the vertical velocity is larger than 0.2 m/s. The mean vertical velocity from the simulations was 0.0076 m/s. For the height from which the package was dropped, the maximum height was 4.7 m, the average was 3.1 m and the minimum was 0.9 m. The total velocity range of the package was smaller with the maximum being 8.4 m/s, the minimum 6.9 m/s and the average was 7.7 m/s. The maximum angle in the simulation was 0.11π, the minimum -0.11π and the average 0.00.

We can now compare the ranges from the simulation to the ranges in Fig. 4.2 and the errors that are expected using the disturbance function. For the drop height, 0.9 m was lower than we expected; however, the height should not result in an error of more than 0.1 m. For the horizontal velocity of the package, the ranges overlap more and we see that once again a maximum of a centimeter error should be expected from this parameter thanks to the disturbance matrix. The error caused by the vertical velocity of the package should be at around 1 cm. Lastly, while the minimum angle is problematic and could cause up to 0.2 m error, the average angle should cause at most a couple of centimeters. This means that we should expect around errors of a couple of decimeters to half a meter between where we think the package will land and where it lands. This is significantly smaller than the error we witness in Fig. 4.24. Here the error of the analytical approximation reaches up

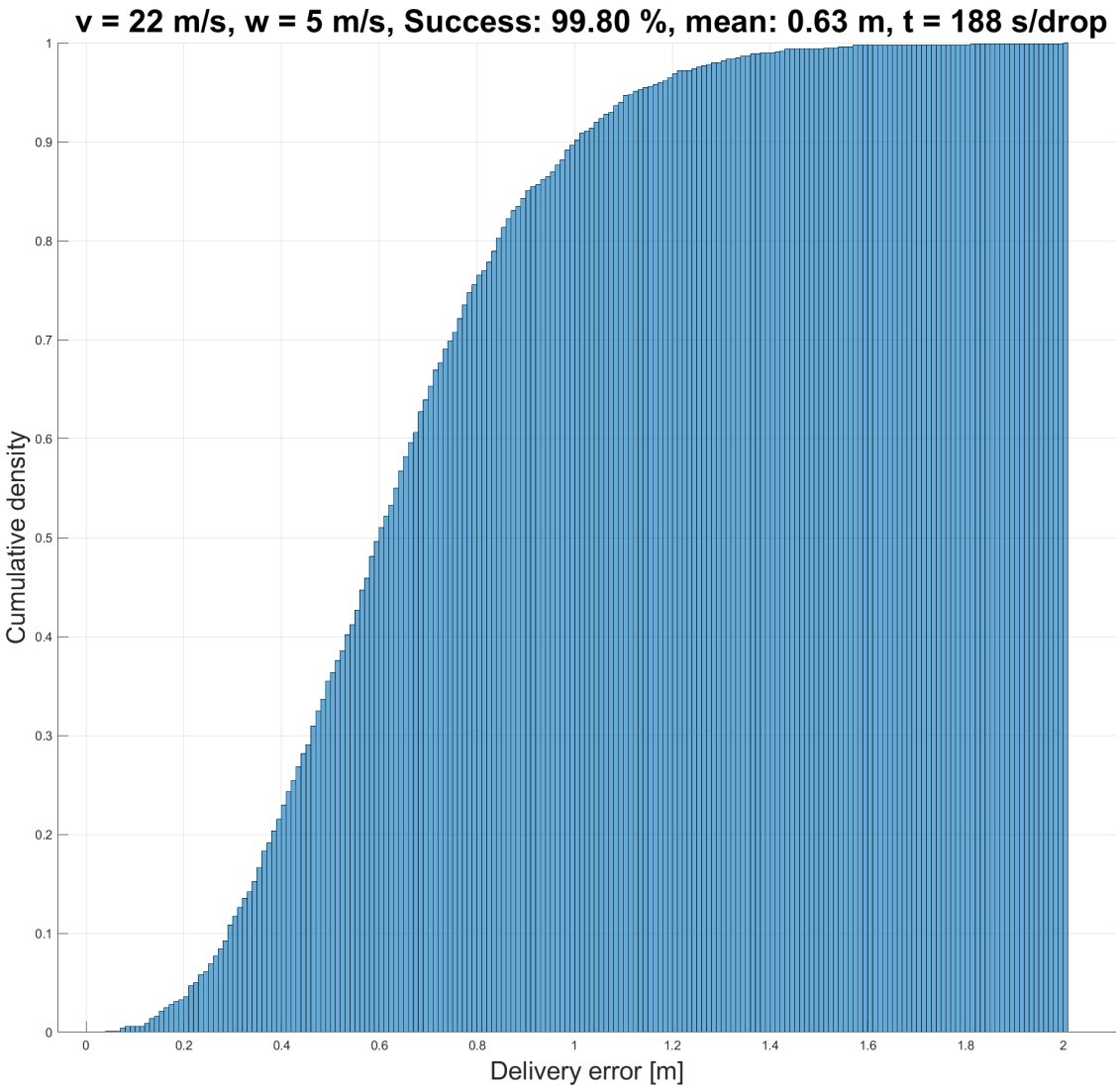

Figure 4.24: CDF for all successful drops for a larger simulation releasing the package with the wind. A total of 1000 simulations were run with the values: drone velocity 18 m/s, rope length 45 m, average wind speed 10 m/s, number of passes 5 and threshold error 0.6 m. The success rate denotes how many attempted drops were successful.

to over 1 m. This suggests that a combination of bad values increase the expected error significantly, or it could simply be caused by the turbulence of the wind.

The last step in attempting to explain why the disturbance function performs worse than without it is to look at the standard deviation for the different values. As we've seen the average values for height and angle are what we want them to be, how much does the other values deviate from said average? The standard deviation values are: 0.21 m/s, 0.60 m and 0.0437π rad for drop height, total velocity and angle respectively. These values could be part of the explanation as to why the disturbance function does not improve the performance, but further study is required.

5
Conclusion

The solution for the package's approximate differential equation system can estimate where the package will land decently well with no turbulence. However, to improve the precision further, a disturbance function can be used. Using more values for the different variables when generating the disturbance function can improve accuracy. However, this comes at the cost of significantly increased memory requirements to store the corresponding matrices, as well as rapidly growing computation time during generation. A significantly larger source of error than the errors stemming from the analytical approximation—even with the disturbance function—is the turbulence. Controlling the environment to ensure the drop occurs under conditions where turbulence has minimal impact is key to achieving high accuracy.

For the fly-by drop algorithm, when maintaining an airspeed for the drone of 20 m/s, the errors are similar whether the package is released headwind or tailwind. An exception is shown for high tailwinds, where a sudden increase in errors are recorded. There is however evidence that indicates this might be due to numerical errors. Releasing the package headwind, the landing velocity of the package is significantly smaller, making this method preferable. However, even for a gentle breeze, the algorithm is not able to consistently land within a target point of 1 m. For a wind size of 7.5 m/s the package only lands within this distance half of the time, a result that is aggravated for higher wind speeds. When it comes to the package's velocity at landing, it is, for headwind drops, similar for all wind speeds in the range [0 m/s, 15 m/s] and sometimes exceed 10 m/s.

Compared to the fly-by, the circular delivery method can get a markedly better accuracy for all wind sizes up to 15 m/s. For example, at 10 m/s the circular delivery method can with a 95 % certainty deliver the package within a meter of the target point, whereas the comparable value for the fly-by is at 4 m. In this same environment, the package had, when landing, a velocity below 8.0 m/s 95 % of the time for the circular delivery method, and below 9.2 m/s for the fly-by algorithm. One drawback that comes with the circular delivery, however, is that it takes longer time before the package is released. From the time when the drone is 50 m away from the target point, the circular delivery method often needs closer to 3 min before the package lands, while the fly-by algorithm could perform the drop in around 10 s.

Overall the circular algorithm can deliver a package within 1 m of a target point with at least 95 % certainty for wind speeds up to 10 m/s while the fly-by cannot. For a larger wind of 15 m/s the accuracy is decreased to 68 % for the circular de-

livery. The following section revisits and answers the research questions outlined in Section 1.2:

- Is it possible to predict where a falling object will land in high wind environments? Can a disturbance function be used to improve the prediction? And how much does turbulence affect the object's landing position?

It is possible to predict where a package will land under high wind conditions, and the implemented disturbance function improves the accuracy of these predictions. However, turbulence is a significantly larger source of error.

- How well do the baseline fly-by and the circular delivery method perform? How do these methods compare?

The prediction can be used to develop both a fly-by and a circular delivery method. While the circular delivery method is more accurate and more reliable than the fly-by method, the circular delivery method is more time consuming.

6
Future Studies

This work has assumed that it is possible to design a robust control system that is able to maintain a stable circular flight path with near constant radius. It also has to be able to handle disturbances from the wind, as well as from the suspended package. To verify the results in this study it is thus necessary to design such a control system, that works with the simulation code, and prove this to be the case.

For the fly-by baseline, it might be possible to improve the algorithm by researching if one can get a more accurate result by being more considerate in what velocity the UAV should target, and how this velocity varies with the wind. One could also study what threshold error gives the most desirable balance of accuracy and release probability. Finally, it would be valuable to verify whether the large increase observed under high tailwind conditions is due to a physical phenomenon or the result of a simulation error.

For the circular delivery, there are a couple of areas that require further research. First, the helical vertical descent function. The simulations needed to test the function are computationally intensive, meaning that each small change to the function requires long computing time to test. The helical vertical descent function was therefore not perfected during this study. While it succeeds at keeping the package at the desired height for the drop, the package still sometimes falls below the zero height line. This is comparable to the package being dunked in the water.

Improvements can also be made to the disturbance function. One can make more considerate decisions as to what, and how many, values to use in generating the function. Is there possibly another disturbance function than the one suggested, that could better counteract the errors caused in approximating the system of differential equations? Or is there a better approximation of the system that gives a better precision in the estimations in the first place?

One part in making the algorithm viable, at least in sea rescue situations, would be to take into consideration that the target may be moving. To be able to handle this, updates to the algorithm are necessary. Also, the coordinates of the target might not be known with high precision. One could instead use camera inputs to update the target point once close to the vessel.

Another assumption made in this report that is not fully realistic, is that the package is assumed to be a perfect homogeneous sphere with a mass and diameter that is

perfectly known. It is safe to assume that real packages will not be perfect spheres, and that the weight and diameter will deviate from what is expected. However, how large an error these discrepancies introduce is currently unclear.

A large area that needs further studies is transforming the problem to the real world. Simulation works up to a certain point, but no matter how carefully the environment is designed, it will never behave exactly like reality. To be able to fully determine the viability of the circular delivery method it is necessary to make tests in a physical space to see how close to reality the simulations get.

Bibliography

[1] Z. Dukowitz. "What are the top uses for drones in 2024? new report reveals trends in commercial drone applications." Accessed: 2025-05-21. (2024), [Online]. Available: https://uavcoach.com/drone-uses-2024/.

[2] A. Käck and O. Wångdahl, "Spiral Drone Delivery," 2022. [Online]. Available: https://odr.chalmers.se/server/api/core/bitstreams/238d6295-789a-415d-8505-0ece76016ed6/content.

[3] B. B. Online, *How are boats measured?* https://www.boatingbasicsonline.com/how-are-boats-measured/, Accessed: 2025-02-11.

[4] S. A. Hsu, E. A. Meindl, and D. B. Gilhousen, "Determining the power-law wind profile exponent under near-neutral stability conditions at sea," *Journal of Applied Meteorology*, vol. 33, no. 6, pp. 757–765, 1994.

[5] "Flying qualities of piloted aircraft," United States Department of Defense, Military Standard MIL-STD-1797A, 1990, Available online. [Online]. Available: https://engineering.purdue.edu/~andrisan/Courses/AAE490F_S2008/Buffer/mst1797.pdf.

[6] MathWorks, *Von kármán wind turbulence model (continuous)*, https://se.mathworks.com/help/aeroblks/vonkarmanwindturbulencemodelcontinuous.html, Accessed: 2025-05-25, 2024.

[7] Lantmäteriet, *Tyngdkraften*, https://www.lantmateriet.se/sv/geodata/gps-geodesi-och-swepos/Referenssystem/Tyngdkraftssystem/Tyngdkraften/, [Online; accessed: 23 maj 2025], 2025.

[8] John Wiley & Sons, Ltd., *Appendix B: International Standard Atmosphere*, https://onlinelibrary.wiley.com/doi/pdf/10.1002/9781118568101.app2, [Online; accessed: 23 May 2025], 2013.

[9] AED Superstore, *2025 AED Comparison Chart*, https://www.aedsuperstore.com/resources/aed-comparison-chart/, Accessed: 2025-05-15, 2025.

[10] Defibshop Australia, *Defibrillators Comparison Chart*, https://www.defibshop.com.au/defibrillators-comparisons/, Accessed: 2025-05-15, 2025.

[11] Swedish Meteorological and Hydrological Institute, *Wind data*, Accessed: 2025-05-13, 2025. [Online]. Available: https://www.smhi.se/data/temperatur-och-vind/vind/wind/71380.

[12] P. Williams and P. Trivailo, "Dynamics of circularly towed cable systems, part 1: Optimal configurations and their stability," *Journal of Guidance, Control, and Dynamics*, vol. 30, no. 3, pp. 753–765, 2007. DOI: 10.2514/1.20433.

[13] R. H. Stewart, "Introduction to physical oceanography," in Texas A&M University, 2008, ch. 4.4: Measurement of Wind, Available online: https://geo.libretexts.org/Bookshelves/Oceanography/Introduction_to_

Physical_Oceanography_(Stewart)/04:_Atmospheric_Influences/4.4:_Measurement_of_Wind [Accessed: 22-May-2025].

[14] SMHI, *Varning för medelvind till havs*, https://www.smhi.se/kunskapsbanken/meteorologi/varningar-och-meddelanden/varning-for-medelvind-till-havs, Accessed: 2025-05-15, 2025.

A

Appendix

A.1 Circular Delivery Plots

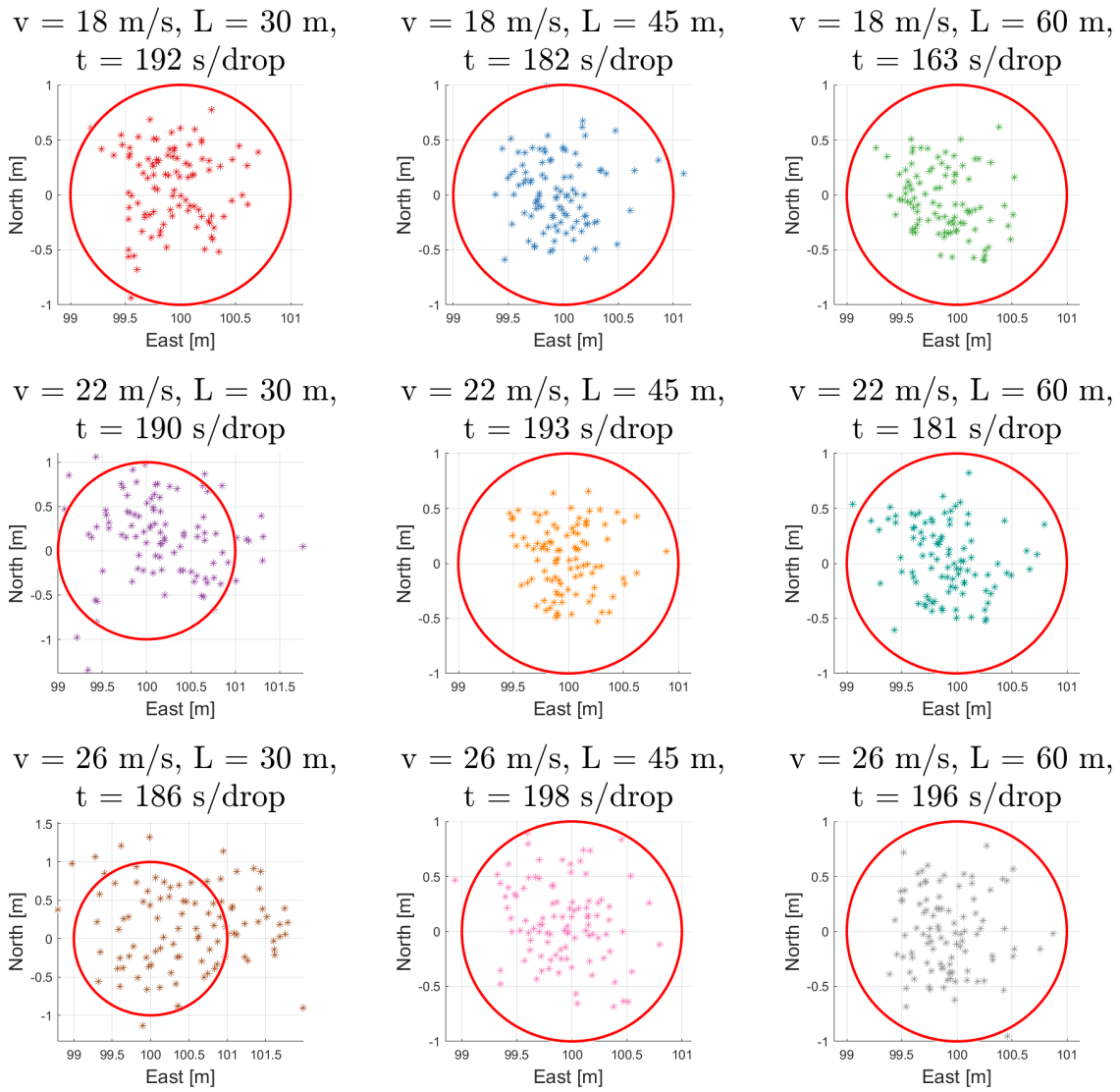

Figure A.1: The landing position for each successful drop for different values of airspeed (v = 18, 22 and 26 m/s) and rope length (L = 30, 45 and 60 m). For each pair of values 100 simulations were run.

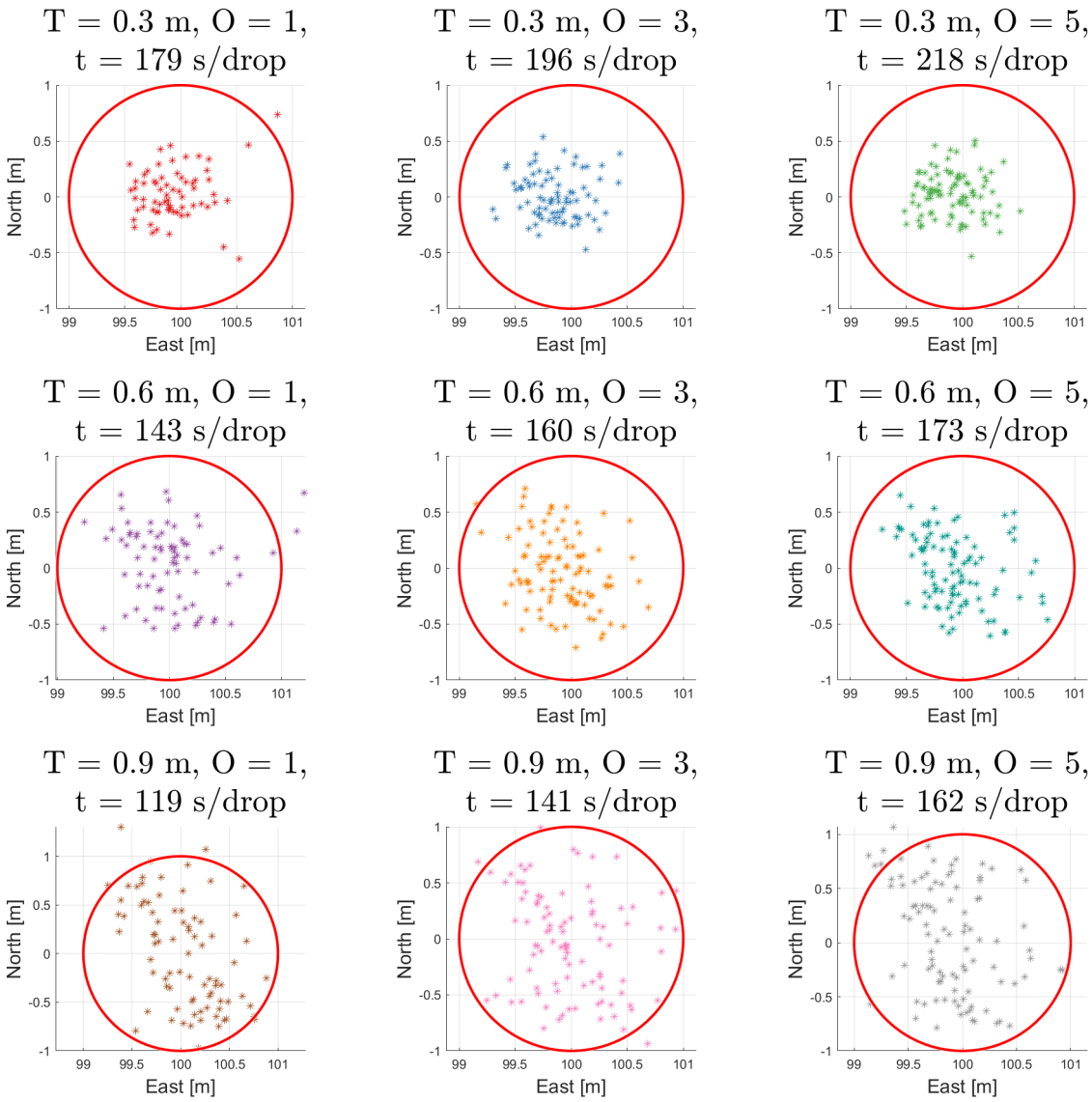

Figure A.2: The landing position for each successful drop for different values of threshold error (T = 0.3, 0.6 and 0.9 m) and offset circulations (O = 1, 3 and 5) For each pair of values 100 simulations were run.

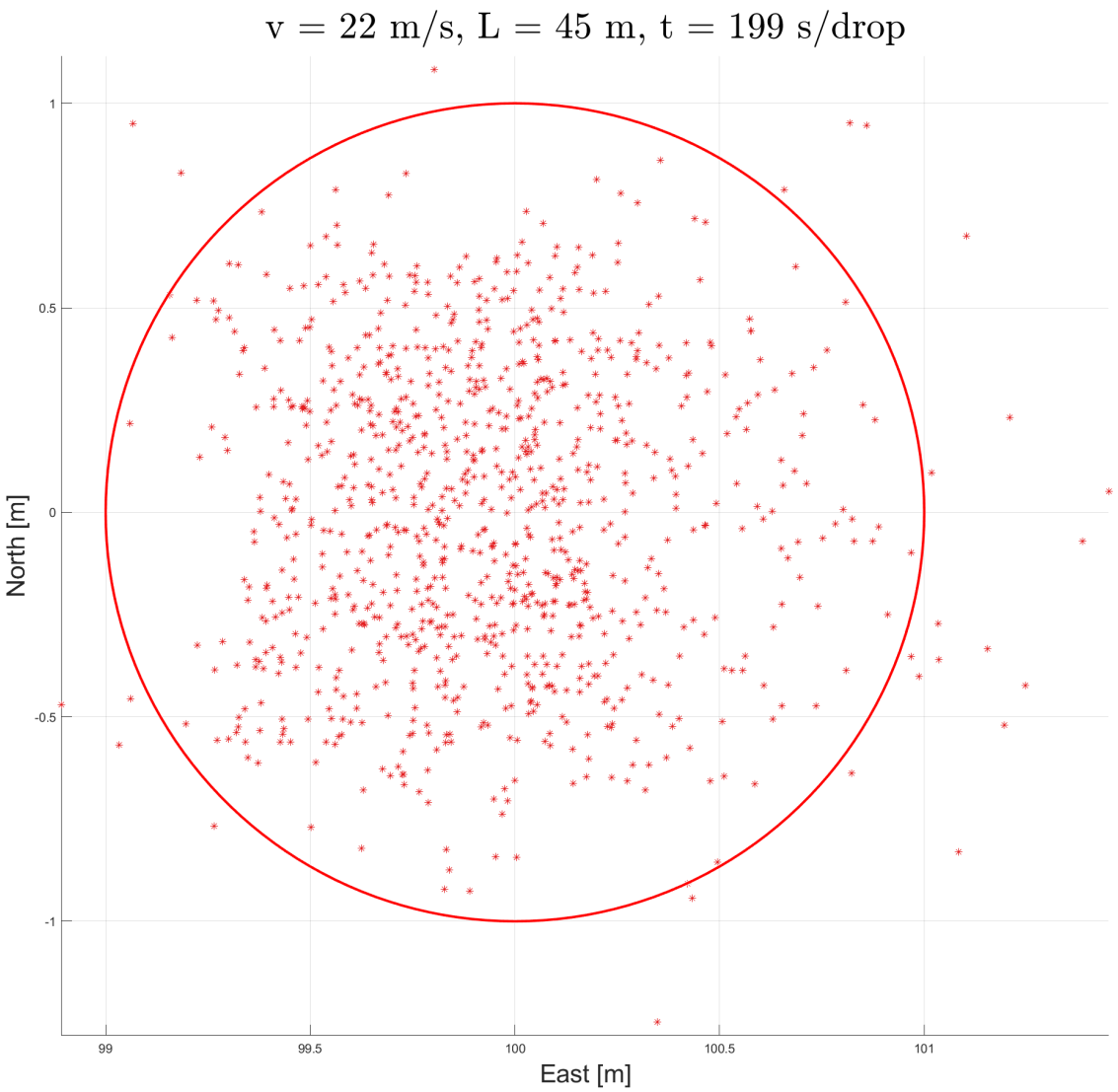

Figure A.3: The landing position for each successful drop for a larger simulation batch. A total of 1000 simulations were run with the values: drone velocity 18 m/s, rope length 45 m, average wind speed 10 m/s, number of passes 5 and threshold error 0.6 m. The red circle denotes the target area with a radius of 1 m.

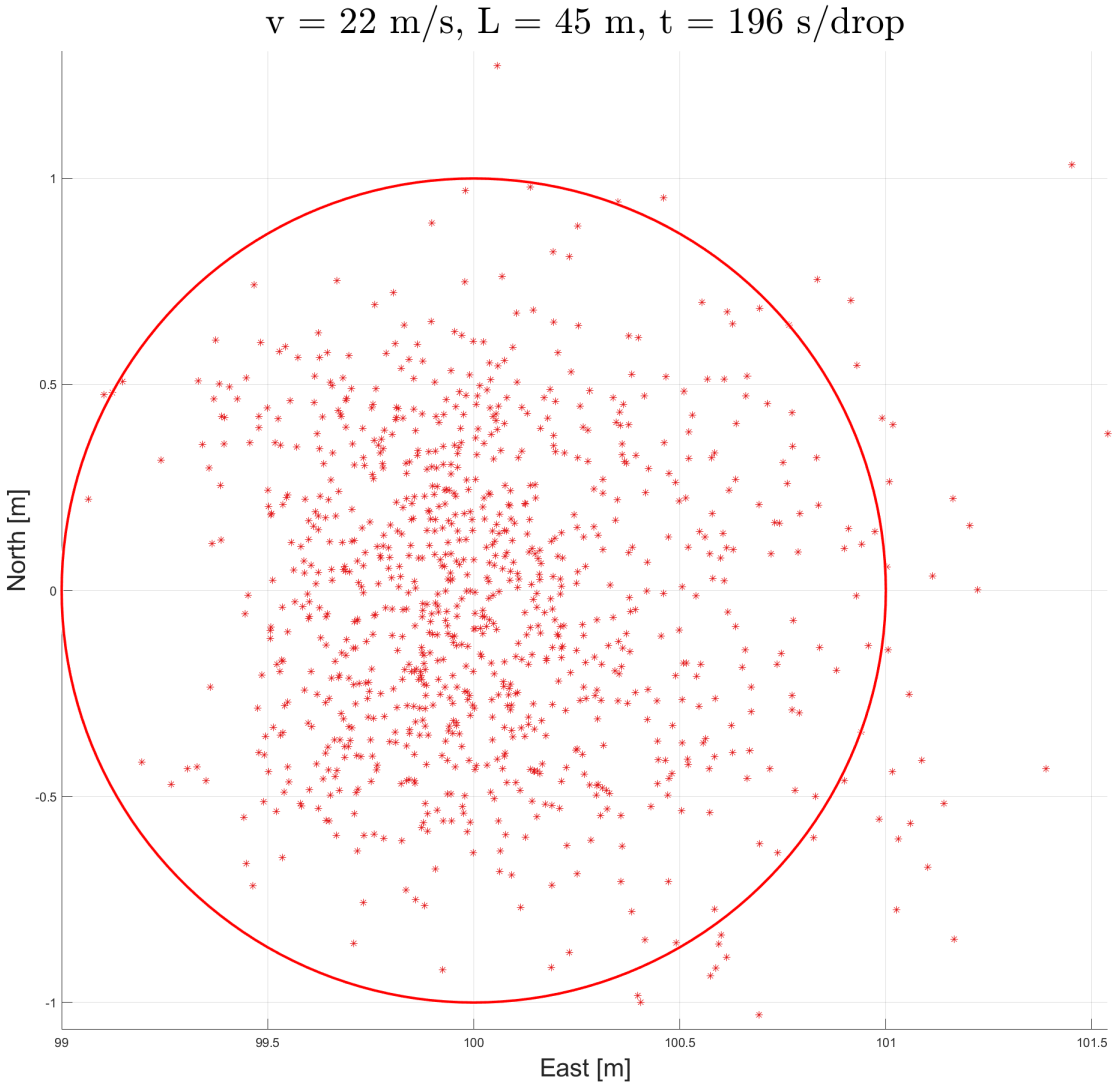

Figure A.4: The landing position for each successful drop for a larger simulation batch using the disturbance function. A total of 1000 simulations were run with the values: drone velocity 18 m/s, rope length 45 m, average wind speed 10 m/s, number of passes 5 and threshold error 0.6 m. The red circle denotes the target area with a radius of 1 m.

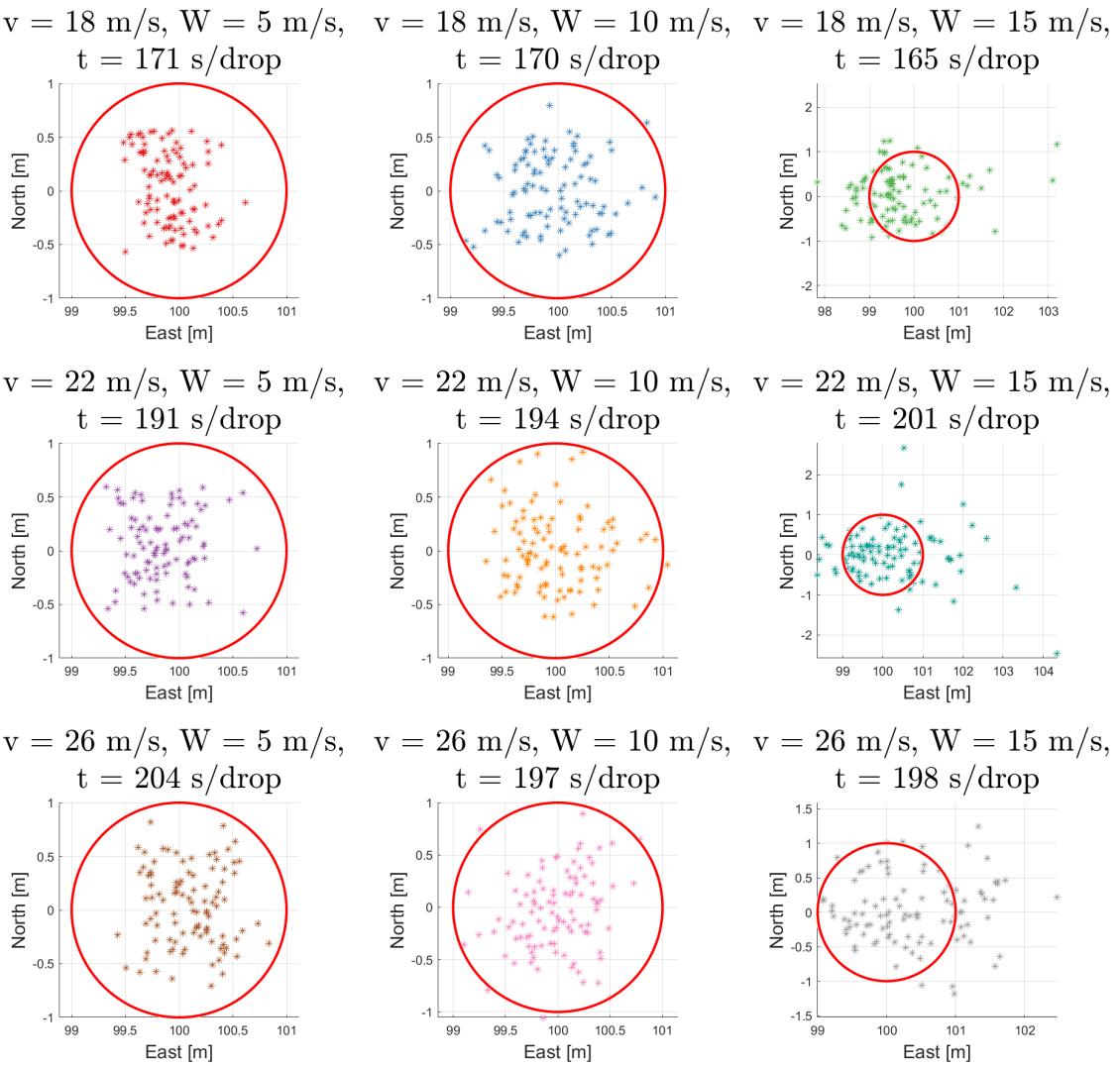

Figure A.5: The landing position for each successful drop for different values of airspeed (v = 18, 22 and 26 m/s) and wind speed (w = 5, 10 and 15 m/s). For each pair of values 100 simulations were run.

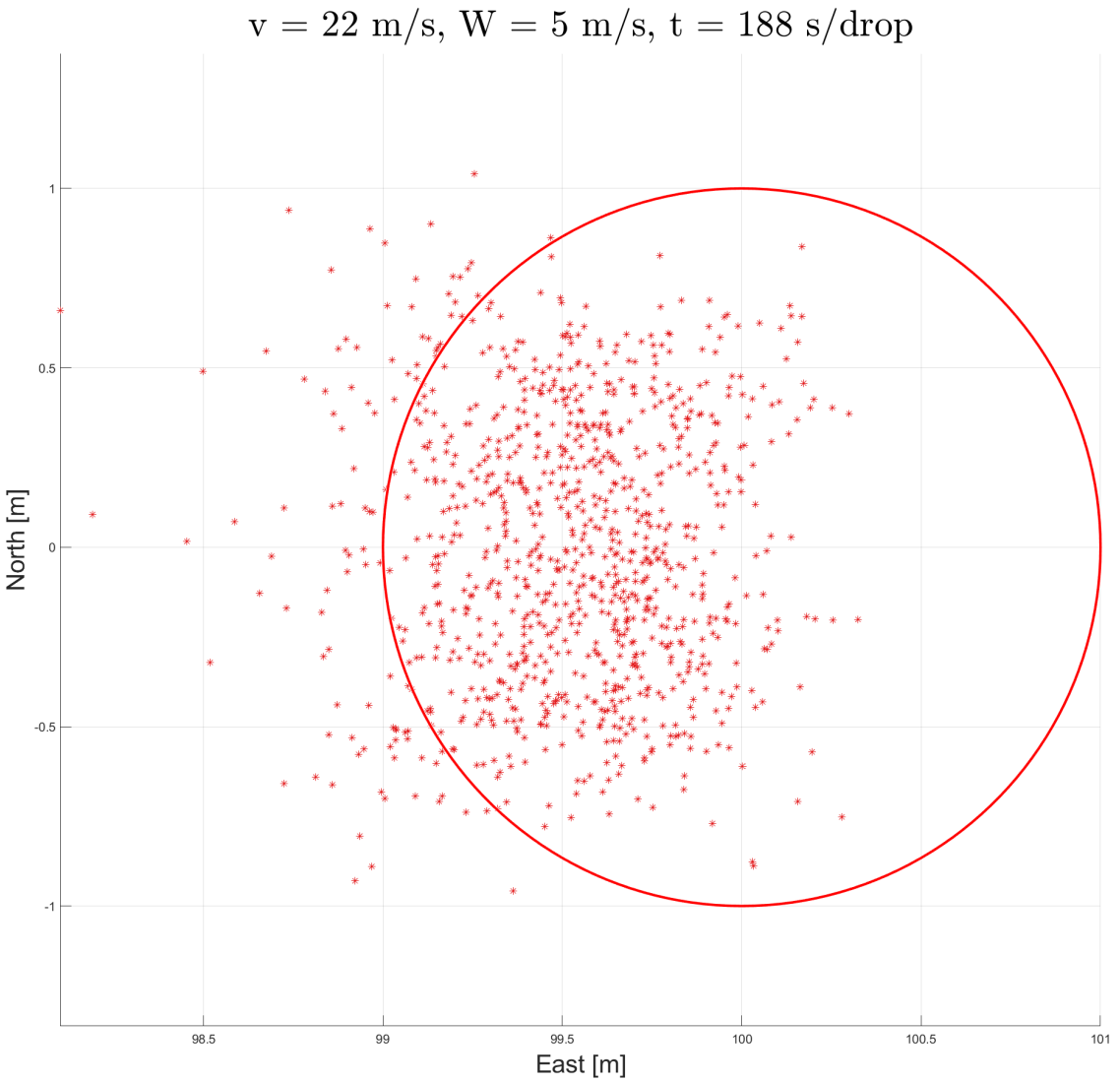

Figure A.6: The landing position for each successful drop for a larger simulation releasing the package with the wind. A total of 1000 simulations were run with the values: drone velocity 18 m/s, rope length 45 m, average wind speed 10 m/s, number of passes 5 and threshold error 0.6 m.

DEPARTMENT OF ELECTRICAL ENGINEERING
CHALMERS UNIVERSITY OF TECHNOLOGY
Gothenburg, Sweden
www.chalmers.se

CHALMERS
UNIVERSITY OF TECHNOLOGY